The Institute of Paper Chemistry

Appleton, Wisconsin

Doctor's Dissertation

Band Spreading in Gel Permeation Chromatography

Neale Page Povey, Jr.

January, 1969

BAND SPREADING IN GEL PERMEATION CHROMATOGRAPHY

A thesis submitted by

Neale Page Povey, Jr.

B.A. 1963, Linfield College
M.S. 1965, Lawrence University

in partial fulfillment of the requirements
of The Institute of Paper Chemistry
for the degree of Doctor of Philosophy
from Lawrence University,
Appleton, Wisconsin

January, 1969

TABLE OF CONTENTS

SUMMARY

Band spreading in aqueous gel permeation chromatography (GPC) was investigated through experimental measurements and through theoretical interpretation of the results. The gels used were Bio-Gel P-2, Sephadex G-10, and Sephadex G-15. The chromatographic system allowed sample injection concurrent with elution and continuous recording of elution curves.

Three diameter fractions were prepared from a quantity of 50-100 mesh P-2 gel. Size fractionation was done by wet screening, then additional fractionations were done by elutriation. Ungraded G-10 and G-15 gels were purified by controlled sedimentation. The particle size distributions of the gel preparations were characterized by extensive measurements with a digital coding microcomparator. The diameters of about 1500 particles were measured for each of the three P-2 preparations and about 1000 from the Sephadex preparations. Computer programs facilitated the reduction of the measurements to five diameter averages plus miscellaneous distribution parameters. The structural swelling behavior of the gels was characterized by measurements of the dry specific volume, wet specific volume, and water regain.

An equation was derived to describe band spreading in terms of measurable operating parameters. The derivations were based on previous theoretical work pertaining to ion exchange chromatography. A significant improvement was made to the theory by modifications which allow predictions to be made at low column efficiencies. Band spreading is described through two independently operating mechanisms: eddy diffusion or multipath dispersion, and slow gel phase mass transport.

The theory was confirmed by measurements of the behavior of two solutes, glucose and raffinose. Three preparations of P-2 gel were used at three temperatures, 15°, 30°, and 45°C.

The height equivalent of a theoretical plate (HETP) was measured as a function of flow rate. The linear relation between these variables was used to calculate an overall mass transfer coefficient, K_L, and a gel phase diffusion coefficient D_g. The relationship between K_L and gel particle diameter was consistent with predictions based on slow gel phase diffusion. There was agreement between gel fractions of the parameter D_g and of the activation energy of D_g.

An analysis of deviations was made to ascertain the proper diameter average to use for theoretical predictions of band spreading. Gel phase mass transport was best described by a diameter average which is equivalent to the most probable volume of the spherical gel particles. A diameter equivalent to the most probable specific surface of the particles was found to describe axial dispersion best – using the random walk treatment of eddy diffusion.

The retardation of solute diffusivity in the gel phase was found to be the most important single mechanism leading to band spreading. This retardation is inherent in GPC systems since the factors which reduce diffusivity are also responsible for solute partitioning. The retardation ratio (gel phase diffusivity/diffusivity in water) was not sensitive to temperature. This ratio had values of 0.067 to 0.0024 depending on the solute and on the gel type. A semilog correlation was found between the retardation ratio and molecular weight for a series of neutral carbohydrates having discrete molecular weights from 92 to 1134. The slope of the regression line is a normalized index of the extent of band spreading for a particular gel type. These slopes were: 6.07×10^{-4} for P-2, 8.67×10^{-4} for G-15, and 15.9×10^{-4} for G-10.

Overlapping of solute bands is to be avoided when a chromatographic separation is designed. Peak separation and band spreading are the two effects which must be considered when approaching the problem. In GPC, peak separations are increased by increasing the degree of cross-linking in the gel, as long as the solutes are not excluded.

Increasing the cross-linking increases the solute-gel interaction, and this results in greater separation between adjacent solute bands. However, this also decreases gel phase diffusivity, which increases band spreading. Therefore, increasing the degree of cross-linking can be a self-defeating approach to the problem as was observed when comparing the behavior of the G-10 and G-15 gels.

INTRODUCTION

In analyses by chromatographic methods, the end results often show the effects of poor separation of components. "Overlapping of bands" is the term applied to liquid column chromatography and this behavior is shown in Fig. 1.

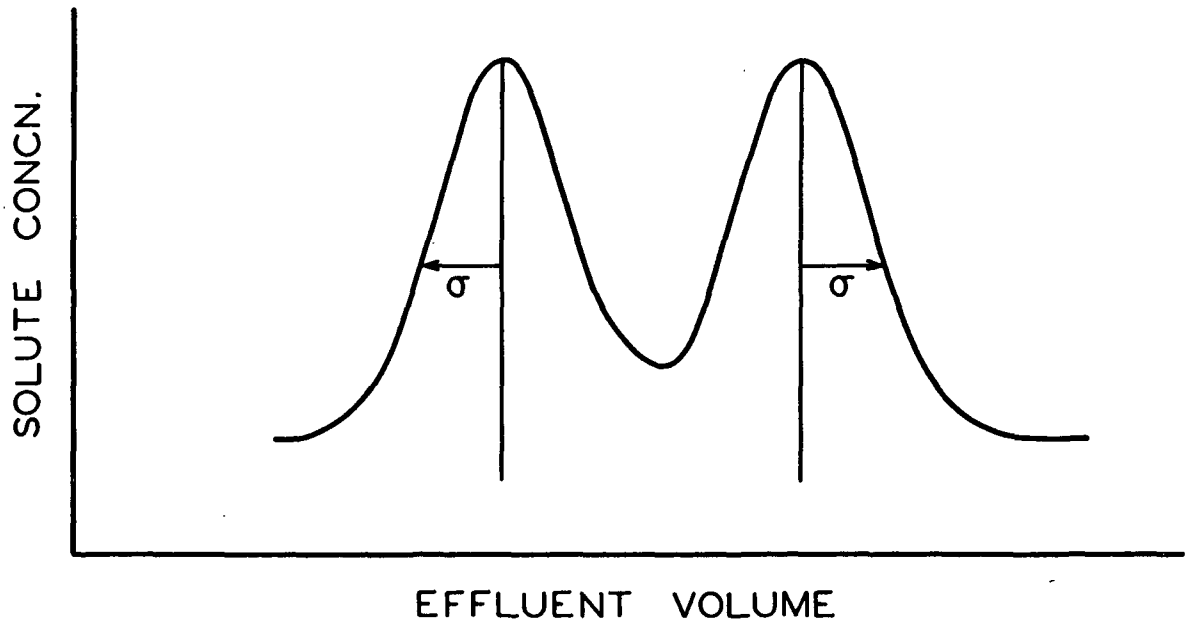

Figure 1. Overlapping Solute Bands

For an ideal separation, each of the components would appear as a discrete peak on the chromatogram. The overlapping region between the two solutes can be diminished by increasing the peak separation, and this is often done by increasing a column's length. Another way to decrease the overlap is to decrease the peak width, indicated schematically in Fig. 1 as σ. The lateral dimensions of a band are determined by more subtle factors than the column length. These factors were studied in this thesis for a particular kind of chromatography – aqueous gel permeation chromatography (GPC). A theory was developed to explain band spreading in this system and experimental analysis was used to examine the theory.

GENERAL CHROMATOGRAPHIC FUNCTION

The objective of chromatographic processes is to achieve separation of molecular components. Separation of components occurs as volumetric or time differences between the emergence of solute entities from a column. Chromatographic columns are operated primarily in two modes which relate to the initial solute introduction – step feed and pulsed feed. Step feed occurs when solute input concentration is initially increased from zero to some finite level and remains at this value for the duration of operation. This is the way industrial ion exchange water purifiers are operated. The plot of effluent solute concentration vs. effluent volume is called a "break-through curve." Pulsed feed is when a small volume of solution is added at the column inlet and this is followed by pure eluting solvent. This mode of operation is most commonly used when a series of components is to be resolved. The resulting concentration vs. volume plot is called a "chromatogram" or an "elution curve."

PARTITION EQUILIBRIUM

All chromatographic systems consist of two principal phases, a mobile phase and a stationary phase. In packed columns the stationary phase is the packing material plus additional fluids which may adhere to the particles or be contained within porous particles. In order to achieve separation, the solutes in a sample must be partitioned in some manner between the two phases. Partition is used here and throughout the thesis in its broadest sense, meaning the distribution of a component between phases. The partition mechanisms vary with the type of chromatography. In GPC the mechanism is not precisely known; however, it involves molecular solution in a restrictive gel network. The molecular mechanisms in GPC will be discussed in greater detail in a later section of the thesis.

If a quantity of column packing is placed in a container with a quantity of binary solution, the bulk solution will become less concentrated until partition equilibrium is established. The functional relationship between solute concentrations is commonly called the solute partition isotherm. The definition of concentration varies and only two of the more common relationships will be discussed here.

In the later derivations the most convenient distribution coefficient is based on the total system volume, i.e., mobile plus stationary phase volumes:

$$k_1 = c_g/c_t \ , \tag{1}$$

where c_g = gel phase solute concentration and c_t = total volume solute concentration. A list of the symbols and their definitions is given in the nomenclature section at the end of this thesis. A specification peculiar to GPC involves the "inner" volume of the gel (1) which is the total volume of the gel minus that occupied by the gel polymer itself.

$$K_2 = \frac{V_e - V_o}{V_{ig}} \tag{2}$$

where

V_{ig} = internal gel volume, V_e = elution volume, and V_o = void volume. This definition of a distribution coefficient is related to one of the theories of partitioning in GPC (2).

The dependence of solute distribution on solute concentration is not simple for many chromatographic systems. Adsorption phenomenon and ionic effects are encountered in many types of chromatography, and factors generally do not lead to simple distribution functions. In GPC, however, a substantial amount of evidence exists which indicates that partitioning isotherms are linear (2, 3) even at high

solute concentrations (4). This behavior is shown in Fig. 2 for two of the solutes used in the experimental work.

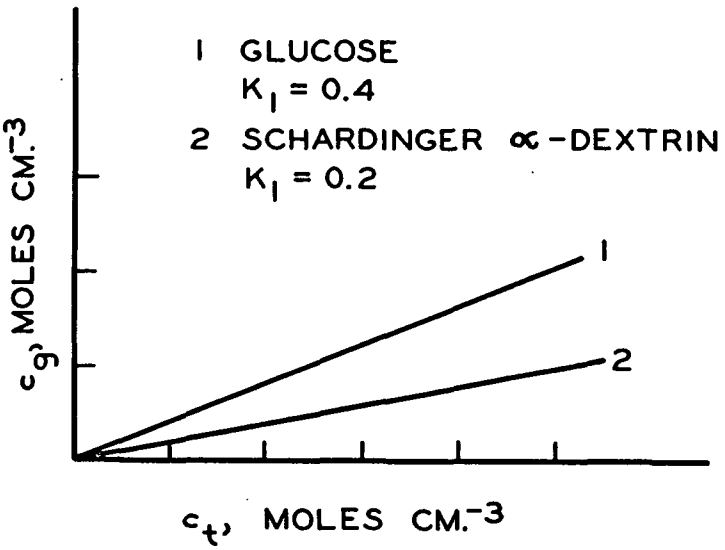

Figure 2. GPC Partition Behavior

As reflected by the slopes in Fig. 2, differences in the solute's distribution coefficients cause the solute bands to move relative to each other as net flow occurs in a column. This results in differing emergence times from a column and is responsible for characteristic peak positions on a chromatogram.

GPC PARTITIONING MECHANISM

The first clear description of a GPC system was given by Lathe and Ruthven (5). Working with partially swollen starch granules, these workers demonstrated that partitioning was due only to differences in the molecular weight of solutes. A commercial product, Sephadex, has recently been made available as a stationary phase for GPC. This material is formed from a glucan polymer by cross-linking in an emulsified state. There are a few other commercial GPC stationary phases

available and these are also produced by emulsion-phase cross-linking. The emulsifying technique produces gel particles which are mostly spherical in shape.

GPC gels used in this study are cross-linked polymer networks which swell in various solvent systems to an equilibrium condition and at this point are considered to be solvated. The interior of the swollen gel consists of regions of solvent and regions of polymer matrix. The relative volume of the regions can be expressed by the gel porosity or by the less fundamental parameter, water regain; a more extensive discussion is given on page no. 27.

A solute molecule moves within the gel network by diffusion in the solvated regions. There are certain spaces that are excluded to solute molecules; these are positions in and near the gel matrix. As a solute approaches one of the forbidden positions, an interaction develops and the approach is limited. The resistances to approach depend on the geometry of the local system — the volume occupied by the solvated molecule and the immediate arrangement of the gel matrix. The driving force depends on the local solute concentration and somewhat on the thermal energy associated with each solute molecule. With larger solute molecules, the interaction occurs at greater distances and the larger molecules cannot enter certain regions of the gel which were accessible to smaller molecules. This is the basis of partitioning by molecular size which occurs in GPC.

With increasing solute molecular size, an increasing fraction of the solvated gel volume is excluded by way of local solute-gel interaction. The same effect is observed when the degree of cross-linking is increased in the gel and the molecular size remains constant. The distribution coefficient for a particular gel-solute depends in part on some molecular volume parameter for the solute and in part on the interior pore geometry in the gel. The functional relationship between these two factors and the distribution coefficient has been the basis of several studies, particularly in the field of polymer-related GPC.

PARTITION RATE

The driving force for transport into a gel is the departure from the local equilibrium condition. In a column this would be the instantaneous gel phase concentration compared to what that concentration would be if elution were stopped and the solute was allowed to come to partitioning equilibrium. The resistance to transport inside the gel can be likened to diffusion in free solvent with three additional mechanisms which tend to decrease the apparent diffusion. First, only the solvated volumes of the gel are available for diffusion. Second, the diffusion paths are more tortuous than in the free solvent. Third, the actual mobility of the solute may be reduced by interactions with the gel matrix.

Partitioning equilibrium is achieved through the driving force and is opposed by the resistances. This necessitates a finite gel-solute contact time for the establishment of equilibrium conditions. In a chromatographic column the equilibrium condition is never achieved. A quantitative formulation of this rate and its effect on band spreading will be discussed in a later section.

SPREADING MECHANISMS

AXIAL DISPERSION

Axial dispersion occurs irrespective of solute partitioning and can be considered as those factors which cause dispersion for a solute which exists only in the mobile phase. Axial dispersion is divided into two effects: longitudinal diffusion and eddy diffusion. Longitudinal diffusion is caused by molecular solute diffusion in the mobile phase. This effect may be dealt with summarily since the data from this work has indicated that the effect can be neglected, and other work (6) has shown that the effect is generally small in liquid column chromatography.

Eddy diffusion is the vague expression used to describe the short-range variations of fluid velocities in a packed column. The expression, axial dispersion, will be substituted with the understanding that the effect referred to has been traditionally called eddy diffusion. The most popular treatment of axial dispersion is statistical-empirical (7). The result of derivations of this type is the equation of the general form

$$H_e = 2\lambda d_p \qquad (3)$$

where

λ = 0.5 to 4.0.

This implies that band spreading is caused by axial dispersion proportional to the particle size, d_p, and dependent in some unspecified way on the packing structure, λ. Serious attempts have been made outside the field of chromatography to define axial dispersion by way of mathematical modeling. The following paragraph is a short review of the work in this area.

Turner (8) considered a capillary model which contained connecting dead volume spaces. Using a sinusoidal feed input, it was possible to evaluate an apparent pore size distribution for a packed column. Aris (9) has refined Turner's model and derived generalized expressions for the Peclet number. These sophisticated models do not give usable predictions for axial dispersion effects in GPC. However, their fundamental approach gives at least an improved qualitative understanding of axial dispersion.

Sherman (10) has investigated axial dispersion in the washing of fibrous beds. Comparing his results with other work on beds of granular material, he concluded that pore size distribution is the factor which predominates in determining the extent of axial dispersion. The definition and measurement of pore size distribution is a difficult task even in ideal situations (11). It is comparatively easy to

measure particle size distributions, but there is no satisfactory correlation between grain size and pore structure.

Pore structure is dependent on the particle shape distribution, on the particle size distribution, and on the spatial arrangement of the packed particles (12). The methods of packing chromatographic columns have varied considerably, and it is reasonable to expect that the particular method will have a strong bearing on the extent of axial dispersion. In evaluating others' work, though, it is difficult to distinguish between effects due to packing structure and effects due to gross irregularities in the bed. A study with silica gel columns indicated that a 20-fold variation in λ can be attributed to packing technique (13). Reproducibility of packing received attention in this research.

RESISTANCES TO MASS TRANSFER

In an operating chromatographic column, solute molecules are continually moving between the mobile and stationary phases. A finite time is necessary for the transport of solute from the bulk fluid to the interior of the gel, and this general nonequilibrium effect causes the spreading of a chromatographic band. The resistances to transport are a combination of hydrodynamic and diffusional factors operating in concert; however, the factors are considered to operate independently for purposes of analysis.

There is a resistance to solute transport from the bulk interstitial fluid to the proximity of stationary particles. At nominal flow rates this resistance is negated by mixing due to short-range randomness in the velocity of the flowing fluid. Experimentally, this effect has been considered and found to be insignificant in most cases (14).

A static film of fluid exists at each of the particle surfaces in a chromatographic column and there is a resistance to solute transport across this film to the particle. The single sphere correlations give unreasonably large film thicknesses at the low Reynolds-number conditions in GPC. Furthermore, any calculations based on film theories would involve significant corrections for the high rates of mass transfer which occur in GPC (15). Carberry (16) has studied boundary-layer models for ion-exchange columns and has obtained transfer correlations from Reynolds numbers of 1 to 1000. Carberry states that the correlation should not be extended to lower flow regimes since boundary-layer development is significant over distances greater than one particle diameter for these conditions. This peculiar behavior at low flow rates has been observed (17). In GPC, Reynolds numbers are typically from 0.001 to 0.1.

When a sphere of gel is directly exposed to a solution, there will be a time dependent penetration of solute molecules into the sphere. The rate of solute transport depends mainly upon: (1) geometry of the particle, (2) some type of concentration driving force, and (3) a diffusional resistance to transport within the gel. A diffusion coefficient for the solute in the gel phase, D_g, is commonly associated with the gel phase transport. Resistance to solute transport of this nature is commonly called slow particle diffusion.

Some simple considerations lead to the conclusion that slow particle diffusion can be expected to be the major resistance to transport, at least for GPC. About 60% of the volume of a column is occupied by gel particles, and in GPC nearly all of this volume is available for solute occupancy. The diffusion rate of a solute is significantly reduced in the gel phase as compared to the mobile phase. A retardation ratio is commonly used in discussing diffusion in gels:

$$\gamma = D_g/D_m \ , \qquad (4)$$

where $\underline{D}_g$ = gel phase diffusion coefficient and $\underline{D}_m$ = mobile phase diffusion coefficient. From the data in this thesis, this ratio has been calculated at 0.07 to 0.01 depending on temperature and solute. A further consideration is that transport inside the gel occurs strictly by diffusion; while outside the gel, diffusion and flow are involved. The effects of "eddy diffusion," in this case, aid mass transport.

MISCELLANEOUS EFFECTS

Chromatography began as an art, and the significance of many experimental conditions is not yet appreciated by some workers in this field. This has made it difficult to ascertain the value of much of the data which occur in the literature.

Experimentally, it has always been difficult to prepare a well-formed column packing. It is difficult even to reproduce packing porosity under apparently identical conditions. One of the more serious problems is with skew zones, where the boundaries of a solute band are not perpendicular to the column axis. The only diagnostic test for this malady is to observe the behavior of a colored solute as it passes down the column; the only corrective procedure is to repack the column. Instability at the interfaces of a solute zone can cause gross variations in fluid speed across the cross section. This phenomenon, called fingering, can vary from slight curve dissymmetry to the occurrence of false peaks, i.e., secondary inflections in the major elution curve.

Proper inlet and outlet port design has been a serious problem in some work. Unless a bed support is less permeable than the underlying media, the incoming eluent or sample will not uniformly enter the bed. A cone-shaped flow pattern will exist from the inlet to a distance where flow becomes uniform across the packing. This entrance effect is analogous to the dispersion of a turbulent fluid

jet. The effect seems to be common and has been interpreted as representative of an open tube parabolic velocity profile along the entire length of packed columnn (18).

Under certain packing conditions, the packing density is less near the column walls than it is near the center of the column. This leads to the phenomenon known as "wall channeling." Wall channeling has been observed to increase with decreasing column diameter and to increase with increasing particle size (19). The effects at the walls can be minimized by packing the column at high particle volume concentrations.

There can be serious apparent band spreading caused by factors not directly associated with the packed column, viz. large dead volumes. Dead volumes cause backwashing of components in the influent and effluent streams, and can cause a marked dissymmetry of an elution curve. Large-diameter tubing on the effluent line and large volumes beneath the exit port are common in poorly designed systems. Large detector volumes often cause apparent dispersion.

Laminar flow in tubes causes dispersion due to so-called "Taylor diffusion." Under certain conditions, this dispersion can be described analytically (20) by

$$\sigma_v^2 = \frac{\pi^2 \, r_o^6}{24 \, D_m} \, L_o \, U \qquad (5)$$

where

r_o = radius of the tube, cm.
L_o = length of the tube, cm.

Although this effect is normally small, Equation (5) shows why effluent tubes should be as short and as narrow as possible.

PLATE THEORY AND HETP

The first quantitative theory of chromatography was the descriptive plate theory of Martin and Synge (21). Their theory was developed from the analogy of chromatography to distillation. A reflux column can be thought to consist of a series of segments in which liquid-vapor equilibrium exists. Likewise a chromatographic column may be conceptually divided into short segments where partition equilibrium exists between the mobile and stationary phases. The length of this short section is called the height equivalent of a theoretical plate (HETP) and is the parameter most commonly used to define band spreading in chromatographic systems. The derivation of the plate theory has been presented in several texts, e.g., (20, 22), and this will not be discussed here. The results of the theory are useful only to the extent that they allow a convenient method for measuring a solute's distribution coefficient and a solute's HETP.

Using the concept of theoretical plates, two equations were derived (21):

$$K_1 = \frac{V_e - V_o}{V_t} \quad , \tag{6}$$

and

$$N = \frac{V_e^2}{\sigma_v^2} \quad , \tag{7}$$

or

$$H = L \frac{\sigma_v^2}{V_e^2} \quad . \tag{8}$$

Equation (6) is equivalent to the earlier definition of a distribution coefficient, Equation (1), and is the basis of experimental measurements. HETP as defined in Equation (8) is not quite accurate; however, the error is small in

many cases and this equation can be used for design purposes. Appendices I and II include a more thorough discussion of the experimental measurement of HETP. The following are two examples which illustrate the concepts of HETP and band spreading.

EXAMPLE 1

Two columns are identical in all respects except that Column 1 is more efficient than Column 2, i.e., $\underline{H}_1 < \underline{H}_2$, and it can be assumed that

$$L_1 = L_2 \ ,$$

$$V_{e1} = V_{e2} = V_e \ ,$$

$$Q_1 = Q_2 \ ,$$

etc.

Then

$$\sigma_1^2 = \frac{V_e^2}{N_1} \ ,$$

and

$$\sigma_2^2 = \frac{V_e^2}{N_2} \ .$$

But $\underline{N}_1 > \underline{N}_2$. Therefore, $\sigma_1^2 < \sigma_2^2$. This shows that when all other factors are equal, band spreading is reflected by an increasing variance of the elution curve.

EXAMPLE 2

Column 1 is cut from the previous example so that it has the same number of theoretical plates as Column 2. This implies that $\underline{L}_1 < \underline{L}_2$, and therefore, $\underline{V}_{e1} < \underline{V}_{e2}$. By definition, $\underline{H}_1 < \underline{H}_2$. Then, since $\underline{N}_1 = \underline{N}_2$,

$$\frac{V_{e1}^2}{\sigma_1^2} = \frac{V_{e2}^2}{\sigma_2^2} \ .$$

Since $\underline{V}_{e1}^{2} < \underline{V}_{e2}^{2}$, it follows that $\sigma_1^2 < \sigma_2^2$. This states that the variance of the band emerging from the first column is still less than the variance from the second column. The point of this is that the number of theoretical plates alone does not give a complete assessment of band spreading.

With distillation, the HETP varies with conditions such as type and concentration of fluids, reflux ratio, loading, etc. Likewise, with chromatography HETP is a function of such variables as flow rate, temperature, solute, and particle size. There is considerable evidence that HETP is independent of column length (23) and is only slightly dependent on initial solute volume and concentration (24).

The plate theories are useful in that they relate measurable quantities to HETP. The plate theories do not relate to the more useful application of predicting band spreading from system parameters. The more sophisticated rate theories are based on mechanistic models instead of descriptive models and, therefore, relate to the fundamental parameters. The rate approach has been used in the following section where a model is developed to explain spreading behavior in GPC.

QUANTITATIVE MODEL FOR BAND SPREADING IN GPC

The behavior of many complex systems such as chromatographic devices cannot be described usefully in an analytical manner. When this situation exists, a simplified model is usually developed and the analytical treatment of the model is then related to the real system. Theories of behavior are improved by making the model conform more exactly to the current conception of the behavior of the real system. In order to develop theories, a precise measurement of behavior in the real system is necessary.

HISTORICAL REVIEW

As discussed in the previous section, the first theory was developed in 1941 (21). Following this, a large amount of work was done in the development of new theories related to adsorption types of chromatography. The development of such theories has been reviewed in several texts, e.g., (20, 22). Gel permeation chromatography was not understood until 1956 and it was several more years before the utility of the process was widely recognized. The common approach to describing GPC behavior has been by analogy to adsorption chromatography. The following discussion has been limited to literature which is concerned with the peculiar features of GPC.

Giddings and Mallik (25) have modified Giddings' generalized coupling theory (26) and proposed this for an explanation of band spreading in GPC. The coupling theory is quite controversial and has had only limited experimental study (27). Sie and Rijnders have proposed that a parabolic velocity distribution in GPC columns is a major source of band spreading (18).

Studies with polymer-GPC systems have been complicated by disperse molecular weight solutes; however, there is a great deal of interest in this area. Smith and Kollmansberger (6) have speculated that mass transfer effects were important in a nonaqueous system. Their analysis was incomplete, though, and a detailed explanation was not attempted. A novel approach has been developed to circumvent the problems which arise when using disperse polymer samples (28). A sample band was eluted halfway down a column, then the flow was reversed. In this way, the resulting chromatogram showed only the effects due to nonideal dispersion. Theories dealing with polymer-related GPC have been concerned with correcting for band spreading and not with the nature of the mechanisms which cause it.

FORMULATION OF EQUATIONS

General equations of continuity and diffusion have been derived for flow through porous media (29, 30). However, ambiguities in the definition of variables and problems with space averaging have limited the usefulness of such equations. A more fruitful approach has been to perform a differential mass balance across a short finite length of column and then to manipulate the equations which result. This has been the method used by most theoreticians (31, 32, 24). All of the results from this approach are essentially the same equations, differing only in numerical constants which refer to geometrical assumptions. The following equation has been ascribed to Glueckauf (24) and his derivation is outlined in Appendix I.

$$\underset{(1)}{\frac{D_m}{U\sqrt{2}}\frac{\partial^2 c_m}{\partial Z^2}} = \underset{(2)}{A\frac{\partial c_t}{\partial V}} + \underset{(3)}{\frac{\partial c_m}{\partial Z}} \qquad (9)$$

Term (1) accounts for longitudinal diffusion and in the case of GPC is negligibly small. Terms (2) and (3) refer to solute accumulation and concentration change due to bulk flow.

This type of equation has been solved for boundary conditions found in GPC, viz. pulsed feed; and the solution has been well described in the derivations which appeared in the appendix to the paper by Hamilton, Bogue, and Anderson (23). A mathematical solution was obtained for a Gaussian solute distribution along the column axis. The variance of this pulse is proportional to the column length and is the sum of two dispersive effects, viz. axial dispersion and mass transfer resistance. Incidentally, the additive properties of these two effects is at the crux of the controversial coupling theory (26). After rearrangement (23) of the general equation (33), the result is given in terms of the variance of a band which leaves the column. Appendix I includes the modifications of this equation which are necessary to allow the application of this theory to the GPC systems used in this thesis. The final form of the equation is

$$H \alpha = \frac{2 D_{axial}}{U} + \frac{2 K_1^2 \varepsilon U}{(K_1 + \varepsilon)^2 K_L} \qquad (10)$$

where

$$\alpha = (1 - \sqrt{2/N})$$

Up to this point the major assumptions have been: (1) Solute partitioning isotherm is linear. (2) Fluid velocity, averaged over ten or fifteen particle diameters, is not a function of position. (3) A zone traveling down the column is Gaussian in shape and the boundaries are reasonably regular. This implies that there are no distortions such as skew zones or fingering. (4) Solutions to the differential equations require that the variance of a Gaussian pulse be moderately long in time. The actual requirements have been stated in terms of column length, etc. (32) and are met in normal GPC operation.

AXIAL DISPERSION

The variable D_{axial} in Equation (10) can be related to measurable parameters. By neglecting molecular diffusion, the Peclet number can be used interchangeably with the commonly used eddy coefficient, λ .

$$N_{Pe} = \lambda^{-1} = \frac{d_p U}{D_{axial}} \quad . \tag{11}$$

The justification for this simplification is based on the random statistical nature of the mechanisms. Helfferich has reviewed the theories dealing with "eddy diffusion" (14), and a detailed discussion will not be given here. Making this substitution for D_{axial} still leaves the ambiguous term λ but the velocity dependency is removed.

MASS TRANSFER

The approach to mass transfer is to specify a linear driving force,

$$N_t = k_L (c_\infty - c_i) = k_g (c_i - \langle c_g \rangle) \tag{12}$$

where

N_t = total solute flux

c_∞ = solute concentration in the bulk interstitial fluid

c_i = solute concentration at the gel/mobile interface

$\langle c_g \rangle$ = average gel phase solute concentration.

The driving forces are then combined using the partition relation, Equation (1), to give the overall mass transfer expression

$$N_t = K_L \left\{ c_\infty - \frac{\langle c_g \rangle (1-\varepsilon)}{K_i} \right\} . \tag{13}$$

In order to relate K_L to measurable quantities, certain assumptions will be made regarding mass transfer. These are as follows: (1) Slow particle diffusion controls the partitioning rate between mobile and gel phases. (2) Transport rate in the gel phase is dependent on a linear concentration driving force. This driving force is the degree to which local concentration is displaced from an equivalent equilibrium condition..

An appropriate gel phase flux equation has been derived (33) and confirmed (34).

$$N_g = \frac{60\ D_g}{d_p^2} (c_1 - \langle c_g \rangle) . \tag{14}$$

The applicability of such an expression for Gaussian pulses has been examined by Bogue (35). This study related to the theoretical consistency of the factor 60 and not to the more general question of whether or not such a model was adequate for real systems. It was found that the flux expression, Equation (14), was satisfactory for long pulses and the approximate limit was determined.

$$\sigma_t > 0.1 \frac{d_p^2}{D_g} \tag{15}$$

where

σ_t = standard deviation of an elution curve, sec.

Returning to the rearrangement of Equation (10), the overall mass transfer coefficient can be replaced by a gel phase coefficient under the stated assumptions.

$$\frac{1}{K_L} = \frac{1 - \varepsilon}{k_g K_1} , \tag{16}$$

or

$$\frac{1}{K_L} = \frac{d_p^2}{60\ D_g K_1} . \tag{17}$$

Using Equation (17), K_L in Equation (10) can be defined in terms of d_p, D_g, and measurable volumetric parameters. Equation (11) can be used to remove the velocity dependence from the axial term in Equation (10). After making these substitutions and after simplification, the resulting equation is

$$H\alpha = 2\lambda d_p + \frac{K_1 \varepsilon}{(K_1 + \varepsilon)^2} \frac{d_p^2}{30 D_g} U . \qquad (18)$$

This equation is similar to those used to describe band spreading in other types of chromatography (22). It is quite simple compared to some expressions used to describe GPC behavior (18, 25) and has been derived in terms of interstitial fluid velocity, U, instead of the usual superficial velocity, U_o.

The factor α is defined in terms of the number of theoretical plates in a column. The derivation leading to this correction is presented in Appendix I. With a system that has 200 theoretical plates, the factor has a value of around 0.9; and when the system is more efficient than this, very little precision would be lost if the correction were neglected. Under inefficient conditions, however, the correction is significant.

Admittedly, Equation (18) represents a simplification of real behavior; and some of the more important assumptions have been described during the derivation. Increased sophistication for the prediction of GPC behavior must be based on experimental evidence so that unproductive speculation can be eliminated. Equation (18) will serve as a basis for comparing observed behavior to that predicted by the simplified model. This analysis of GPC behavior will be carried out in later sections dealing with experimental results and interpretations.

EXPERIMENTAL SYSTEMS

Commercial GPC gels were fractionated according to particle size. The gels were characterized by extensive particle size measurements and by investigation of their hydration properties. The chromatographic column was of an advanced design which allowed continuous injection and elution of samples. Solute concentration in the column effluent was continuously measured and recorded.

GELS

CHEMICAL COMPOSITION

Bio-Gel is a product of cross-linked copolymers of acrylamide and methylene bisacrylamide. Acrylamide forms the backbone of the gel, while the difunctional monomer acts as the cross-linking agent.

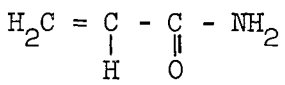

Acrylamide

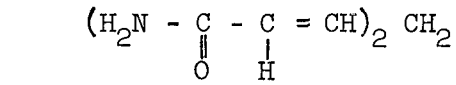

Methylene Bisacrylamide

The process of making Sephadex brand dextran gels has been described by Flodin (4). The native dextran is a high molecular weight polysaccharide formed by the action of a strain of Leuconostoc mesenteroides on sucrose. The GPC material is formed by cross-linking the polysaccharide while the system is in an emulsified state.

Ideally, there is no adsorption involved in partitioning of solutes in a GPC system and this has been found to hold for most proteins and carbohydrates. Aromatic compounds have been found to exhibit adsorption partitioning on dextran gels (36) and a few studies have been made by applying this function to ligninlike compounds (37, 38). Strongly basic salts degrade dextran gels and these compounds

have been found to adsorb irreversibly onto the acrylamide gels (39). Strong adsorption has been found in certain nonaqueous GPC systems, but this can be negated by changing the solvent system (40). In this thesis work, it was found that all common colored substances (pH indicators, Sephadex Blue Dextran 2000, ink) were adsorbed on Sephadex G-10 and G-15 gels. Most of these substances were adsorbed on Bio-Gel P-2 with the exception of Na-bromthymol blue (Sargent) and murexide (Polysciences). These compounds were very useful for the visualization of the eluant flow pattern in the packed columns.

MICROSCOPIC COMPOSITION

The gel fractions were examined extensively at about 40X magnification during particle measurements with the digital coding microcomparator. The Bio-Gel P-2 fractions were further examined and photographed with a Zeiss photomicroscope. It was found that about 10% of the Bio-Gel material occurred as flocs of two or three particles. As shown in Fig. 3, some of the particles are partially coalesced into semicontinuous arrangements. This fusion occurred during the formation of the material, probably of too high a dispersed phase concentration in the emulsion polymerization process. A cursory examination of the Sephadex gels indicated that this material was present as individual spherical particles. As shown in Fig. 4, there appears to be a skin splitting on many of the particles. This lack of mechanical integrity is probably due to a loss of elasticity which accompanies the high degree of cross-linking in these gels (41).

As shown in Fig. 3 and 4, there appear to be discontinuities in both types of gels. On the Bio-Gel particles it appears that the surface is pitted with small depressions. This general type of flaw in cross-linked polymers is well known and has been described in the literature (42-44).

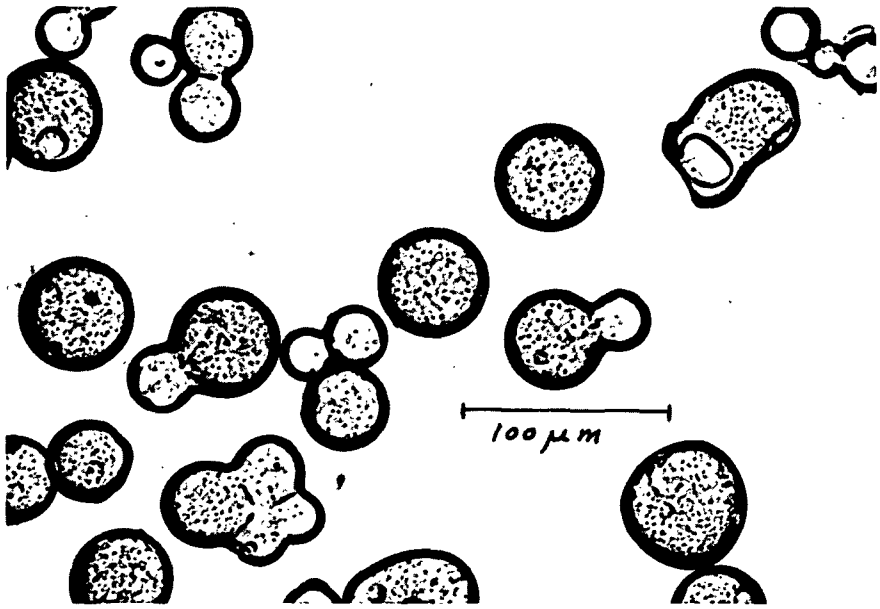

Figure 3. Bio-Gel P-2 Particles, 560X

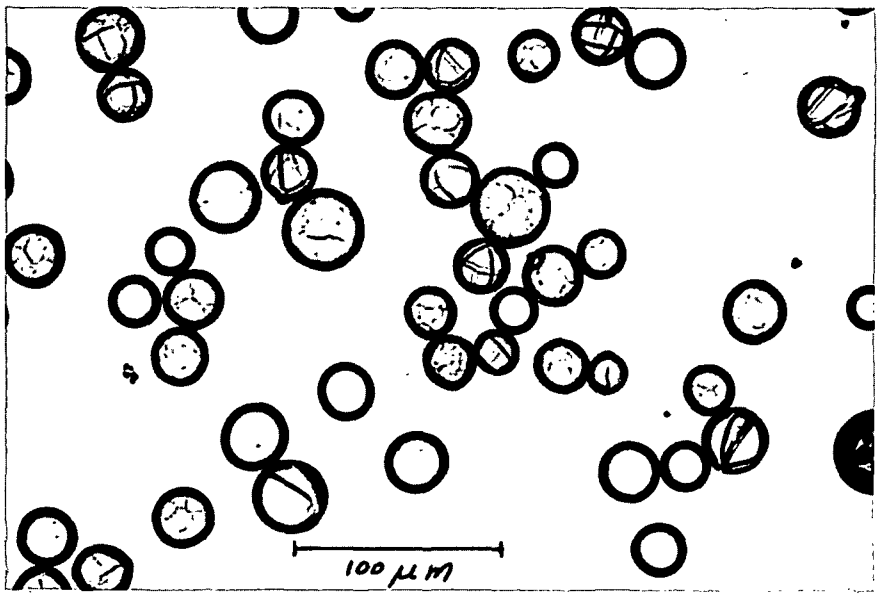

Figure 4. Sephadex G-10 Particles, 560X

The conclusion drawn from the microscopic examinations of the GPC gels is that the material should behave essentially as a continuous gel. The volume occupied by the flaws is small compared to the overall gel volume — an estimated 5-10% of the volume for the Bio-Gel material and considerably less for the Sephadex gels. The particles were not porous in the usual sense since the discontinuities were not interconnected to give channels through the material.

HYDRATION BEHAVIOR

Gels used in GPC are commonly characterized by the water regain as defined in Equation (19). Two additional parameters were estimated in this work as defined by Equations (20) and (21), the wet specific volume and the dry specific volume.*

$$w_r = \frac{\text{grams of hydration water}}{\text{grams of dry gel}} \tag{19}$$

$$\bar{V}_w = \frac{\text{volume of hydrated gel, cm.}^3}{\text{grams of dry gel}} \tag{20}$$

$$\bar{V}_d = \frac{\text{volume of unswollen gel, cm.}^3}{\text{grams of dry gel}} \tag{21}$$

The water regain of chromatographic gels is usually measured by the centrifugal method (45) which has been critically reviewed (46). The water regain of the Bio-Gel P-2 used in this work was measured by two new techniques. Sephadex G-10 and G-15 gels were characterized only by the simpler filtration method. The following is an outline of the methods.

Excluded Solute Method

A quantity of Sephadex Blue Dextran 2000 was dissolved in water, and the concentration was brought to about 375 μg./ml. A measured volume of this solution

*The numerators in Equations (20) and (21) do not include the interstitial volumes.

was added to several weighed samples of the dried gel, and the gel was allowed to swell to equilibrium. The swollen gel and the bulk solution were separated by filtration, and the solution's absorbance at 600 nm. was measured. Blue Dextran 2000 was excluded from the gel, and therefore there was an increase in the color (absorbance) when the dry gel was swollen with a solution of this polymer. The water regain was calculated from the equation

$$w_r = \frac{V_s \rho (1 - c_o/c)}{m_{gel}} \quad , \tag{22}$$

where

V_s = initial volume of solution added, $cm.^3$

ρ = density of water, $g.\ cm.^{-3}$

m_{gel} = mass of dry gel, g.

c_o = initial concentration of Blue dextran, μg./ml.

c = final concentration of Blue dextran, μg./ml.

The initial and final concentrations were calculated from an experimental plot of concentration versus absorbance.

Dental Dam Method

Common filtration and centrifugation methods are inexact due to an incomplete removal of pore water. To circumvent this, filtration was combined with vacuum distillation. A weighed quantity of dried gel was swollen in water and then washed into a tared sintered-glass filter crucible. The bulk of the pore water was removed with suction, and then the vacuum was continued with a piece of dental dam fastened over the filter. The dental dam acted as a flexible barrier, and all of the gel was subjected to a vacuum determined by the vapor pressure of the tap water which operated the air ejector.

The mechanisms of water removal can be seen by referring to Fig. 5 where water loss is plotted against time of filtration. Data points are an average of three determinations. The apparent behavior is a rapid loss of pore water followed by a slow loss of hydration water. Weighings were made after about 20 minutes which corresponds to the transition from pore water removal to hydration water removal. Water regain (Table I) was calculated directly by using Equation (19).

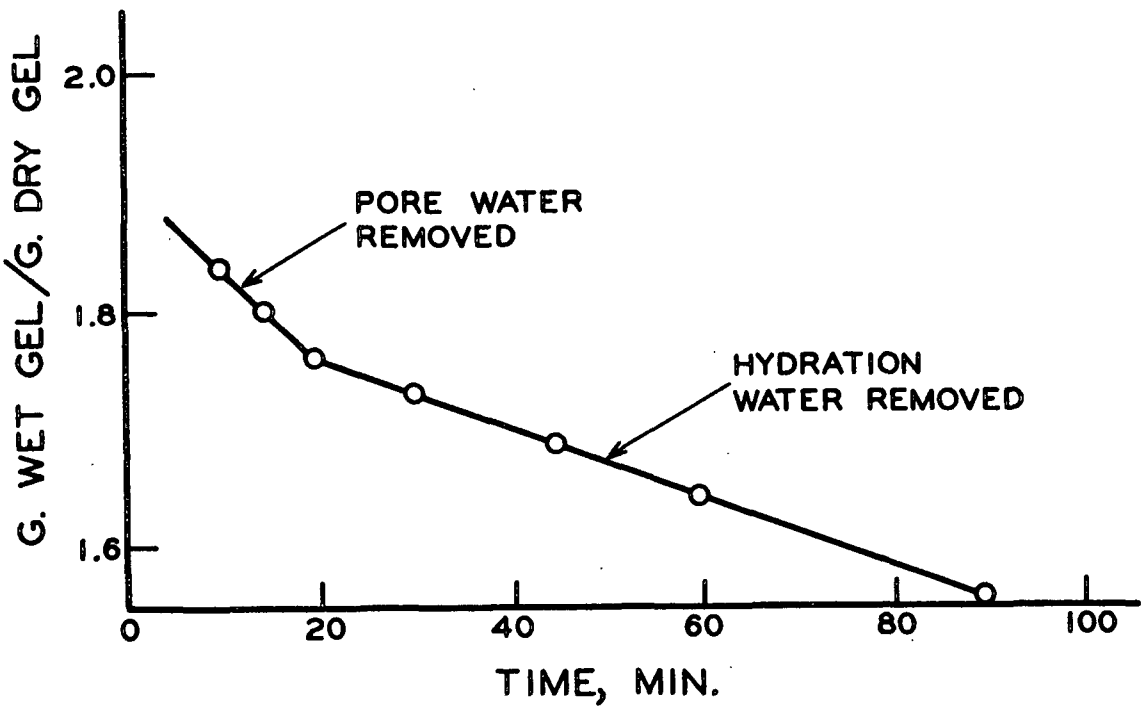

Figure 5. Water Loss During Dental Dam Filtration

TABLE I

WATER REGAIN DATA

Gel Type	Water Regain, g. H_2O g. o.d. gel	Average Deviation
Bio-Gel P-2 (excluded solute)	1.40	0.04
Bio-Gel P-2 (dental dam)	1.38	0.04
Sephadex G-15 (dental dam)	1.21	0.03
Sephadex G-10 (dental dam)	0.79	0.02

As shown from these data, the difference between the two methods was small compared to the experimental error. The reproducibility of the methods was comparable or better than the methods currently employed (45, 47).

Specific Volumes

The specific volumes were determined by repeatedly measuring the sedimented gel volumes in graduated cylinders. The porosity of 0.47 for random loose arrangements (48) was used to correct for the pore volumes. Table II shows the experimental data and the calculated internal porosity of the gel.

TABLE II

GEL SPECIFIC VOLUME DATA

Gel	$\bar{V}_w$	Average Deviation	$\bar{V}_d$	Average Deviation	ε_g
P-2	2.01	0.023	0.994	0.008	0.506
G-10	1.21	0.006	0.952	0.023	0.215
G-15	1.63	0.011	0.869	0.011	0.466
G-25	2.47	0.020	0.663	0.005	0.731

GEL PARTICLE SIZE CLASSIFICATION

The primary chromatographic gel used in this work was a commercial grade of polyacrylamide gel, Bio-Gel P-2. One kilogram of 50-100 mesh gel from lot no. 45152 was fractionated according to particle size, first by wet screening in a Bauer-McNett fiber classifier and then in an elutriation column.

WET SCREENING

Bronze screens of U. S. Standard sieve cloth were soldered to the frames from a classifier, and these were used in all the wet screening work. A two-stage water filter was plumbed to the classifier. The first stage was a 20 cm. "Ful-Flo" cartridge filter and the second was a 142-mm. Millipore filter holder used with disks of Whatman No. 1 filter paper. Demineralized water was used throughout the work.

Fractionation of the gel was begun using coarse screens in the first three compartments, viz. 45, 50, and 60 mesh, and then a 150-mesh screen in the last compartment. The first compartment was loaded with the equivalent of 100 or 200 g. of dry gel, and the classifier was allowed to operate for three to six hours. The water flow rate was not controlled by the usual constant head device, but was regulated by a throttle valve. At the end of the running time, the gel remaining in each of the compartments was collected. The gel was isolated by filtering the slurry through a coarse sintered-glass funnel which was connected to a thirty liter vacuum bottle. Corresponding screen fractions between runs were pooled.

After all of the gel had been subjected to fractionation, the screens were changed adding the next finer mesh. For example, the configuration of 45, 50, 60, and 150 mesh was changed to 50, 60, 70, and 150 mesh. The remaining gel (minus 45 mesh) was reprocessed through the new configuration of screens. By extending

this scheme, the original material was divided into several groups depending on the amount retained in a given screen compartment. The yields from the overall wet screening are shown in Fig. 6.

The decision was made to utilize the gel from the 50-60, 70-80, and 100-120 mesh fractions. There was sufficient material in these fractions to fill the chromatographic column, and each fraction was separated from the next by one unused fraction. These three fractions were washed free of debris and further fractionated by processing with an elutriation system.

ELUTRIATION

Several hydraulic methods were considered and rejected (22). The main difficulty in the methods was in achieving uniform flow at the entrance and exit ports. The system shown in Fig. 7 was designed and built to meet the needs of this work. The entrance to the column consisted of a diverging cone cut in a large rubber stopper. Three circles of 30-mesh bronze screen were fastened into the cone with epoxy resin, and the top of the cone was covered with 200-mesh nylon cloth. This entrance configuration acted as an efficient flow spreader to disperse the upward flowing stream of water. The filter holder also acted as a bubble trap. Effluent from the column was passed through a two-stage sediment collector before entering the pump reservoir. The collectors were 1000-ml. vacuum flasks with influent diverters which were fabricated from glass tubing.

Elutriation is most effective when the particle concentration is low so that a given particle can move independently of its neighbors. As an arbitrary limit, the gel volume concentration in the column was calculated so that there was an average of two diameters separating each particle. A cubic arrangement of spheres was assumed with each sphere separated from its neighbor by two diameters. From the geometry of this system, the void and solid fractions allowed calculation of the optimum gel concentration, about 70 ml. of sedimented gel.

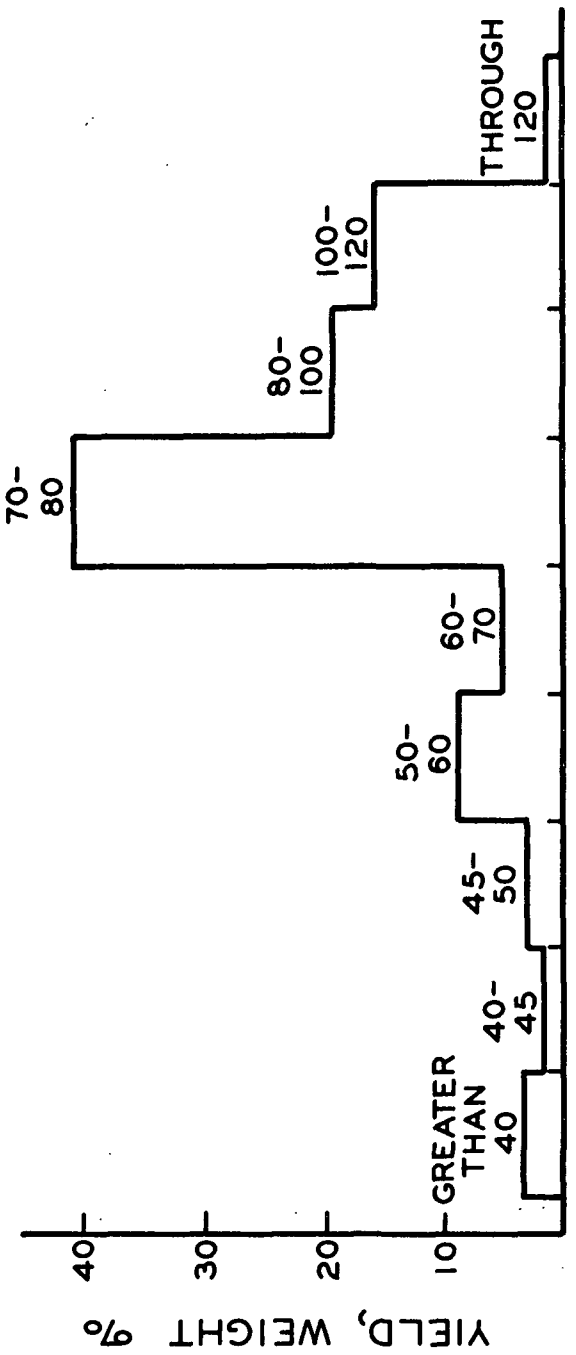

Figure 6. Results of Bauer-McNett Wet Processing

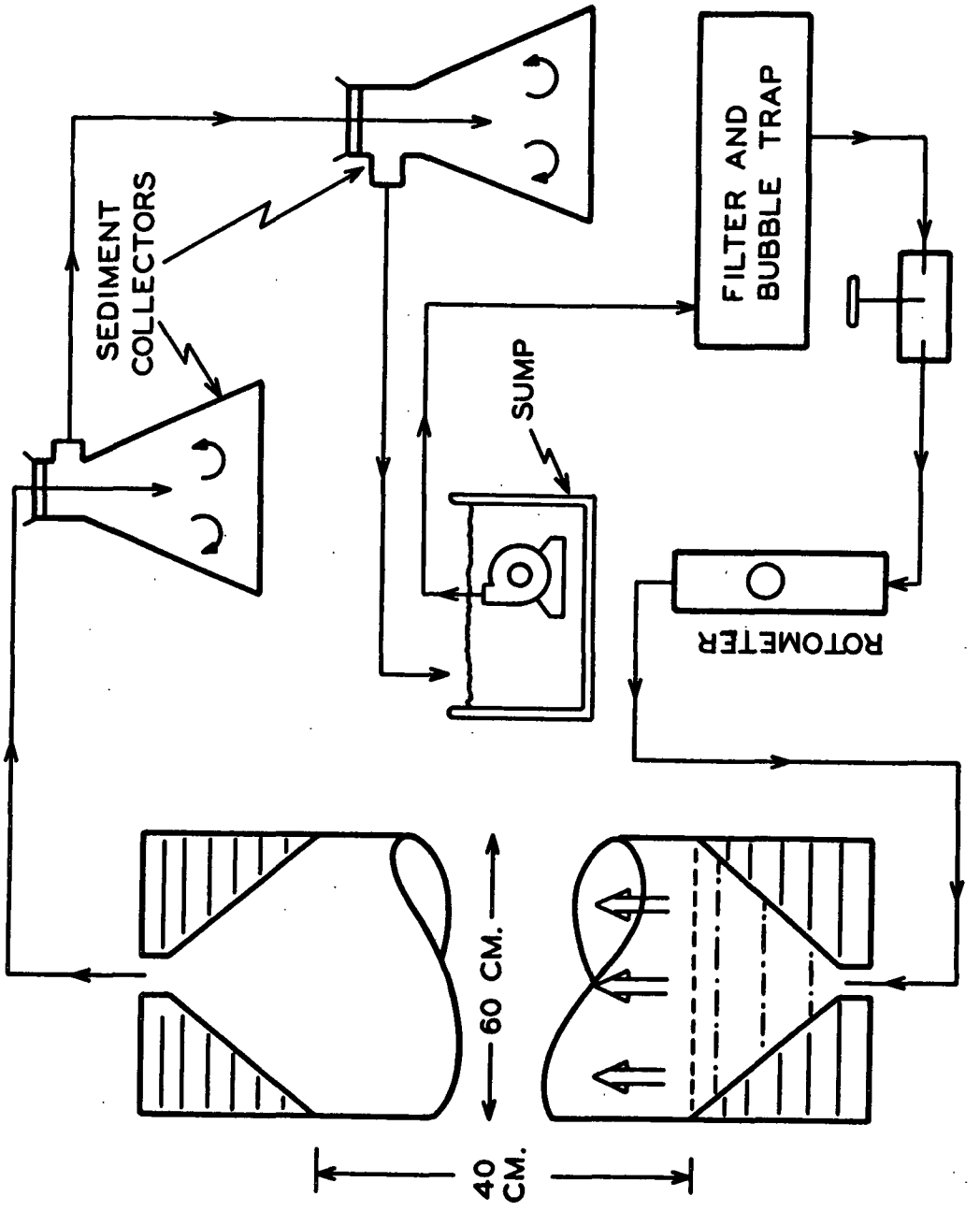

Figure 7. Elutriation System

To check the efficiency of the elutriation process, 70 ml. of sedimented gel from the 70-80 mesh screen fraction was processed and analyzed. A slurry of the gel was poured into a graduated cylinder until the sedimented volume was at 70 ml. The gel was then washed into a vacuum flask and subjected to high-speed mixing for about ten seconds. The slurry was then deaerated using the vacuum from a water ejector. The slurry was poured into the column, and elutriation was increased slowly until the gel was distributed throughout the column. After a time a small quantity was carried out of the column. An estimated 20 ml. of gel was collected, and the flow was stopped. The two fractions obtained were analyzed by measuring 250 particles from each sample. The results of this analysis are shown in Table III.

TABLE III

ANALYSIS OF ELUTRIATION FRACTIONS

	Through the Column	Remaining in the Column
Diameter, $\underline{d}_{\underline{n}}$, μm.	100	126
Diameter, $\underline{d}_{\underline{wv}}$, μm.	111	143
S.D., μm.	35	49

The gel in the three screen fractions was processed as previously described except that three elutriation fractions were taken, the central fraction being largest and consequently used as packing for the experimental work. The elutriation gave three purified gel diameter fractions, each consisting of about 300 ml. of gel.

SEDIMENTATION

Two dextran gels, Sephadex G-10 and G-15, were also studied. These gels were purified by repeated sedimentation followed by siphoning. About 200 g. of each gel was allowed to swell overnight in water. The gel was then deaerated with vacuum and washed into a two-liter Erlenmeyer flask. The flask was filled with water, the gel was stirred briefly with a glass rod, and a 20 cm.-long siphon of glass tubing was placed into the gel slurry. Gel particles were allowed to settle for five and one-half minutes, and the siphon was started removing the top portion of the slurry which contained only particles of diameter smaller than some limit. This process was repeated about 15 times for both of the gel types.

CHROMATOGRAPHIC SYSTEM

The system shown in Fig. 8 was used in the measurements of band spreading. The eluant was distilled water which had been deaerated and filtered through an 8 μm. Millipore filter prior to use. All solutes were commerical preparations and were purified by filtration of the solutions with Darco G-60 activated carbon. The dextran preparation was Sephadex brand Dextran 10; glucose and sucrose were Mallinckrodt AR grade sugars; raffinose, C. P. was obtained from Pfanstiel Laboratories as the pentahydrate. Schardinger alpha-dextrin was obtained from Koch-Light Laboratories, and Schardinger beta-dextrin was obtained from Pierce Chemical Company.

ARRANGEMENT AND OPERATION OF EQUIPMENT

Eluant was first drawn through a deaeration device which consisted of a heating vessel and a bubble trap. The eluant pump was a Sigma Motor peristaltic pump driven through an infinitely variable (Zero-Max) speed reducer. The pump tubing was used either as a single tube or as a duplex manifold to reduce pulsations.

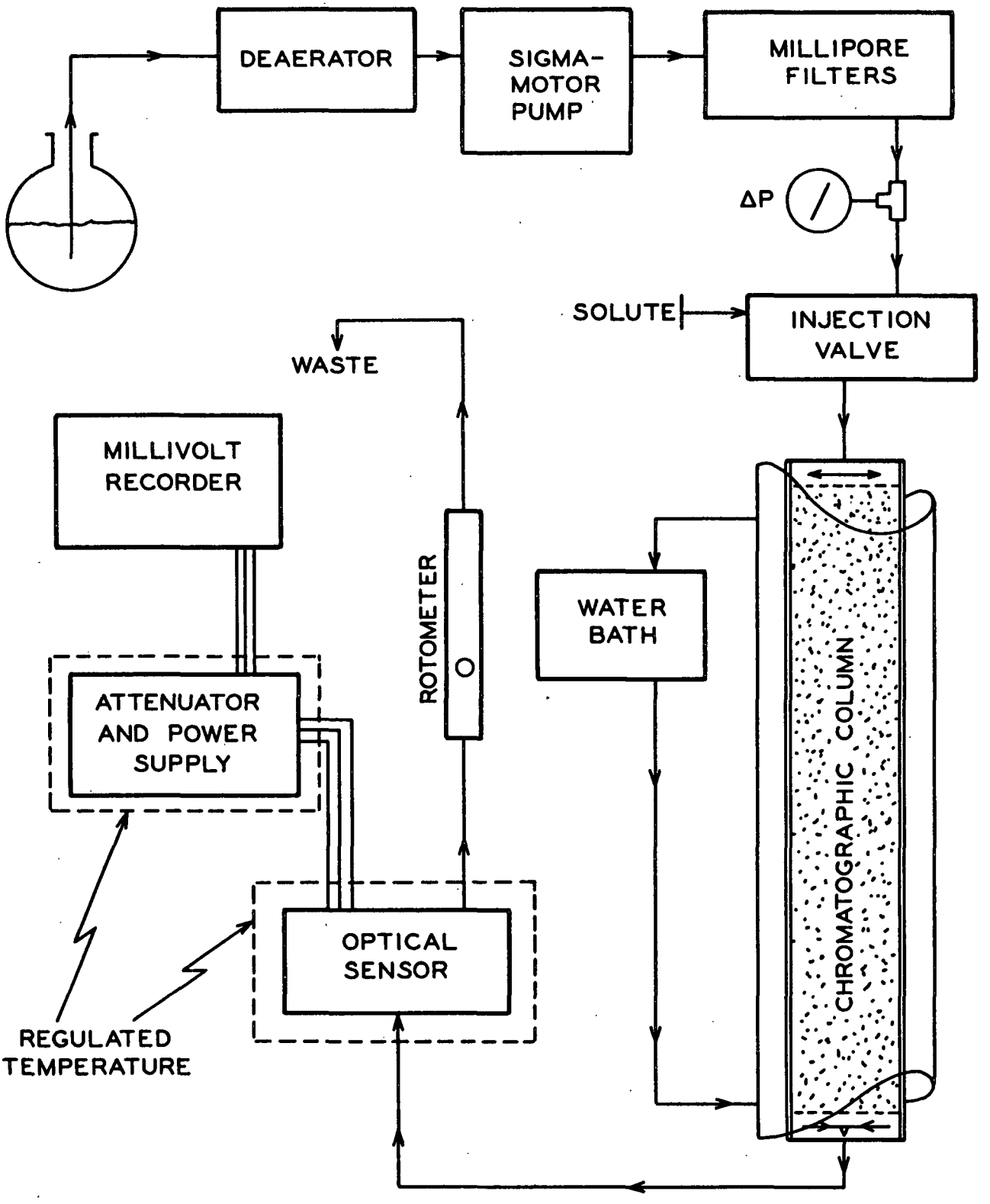

Figure 8. Chromatographic System

The tubing was either polyurethane (Sigma) or Tygon formula S 50 HL. After the pump, the eluant was carried in Chromatronix brand T063031 teflon tubing, and this was used throughout the system until after the optical head of the detector. From this point, Tygon tubing was used.

The eluant was passed through a 47-mm., 8-μm. filter and a 12-mm., 3-μm. filter before entering the Chromatronix model SV-8031 sample injector valve. The construction of this valve is such that flow was not stopped to the column during sample injection; the sample was drawn into a calibrated loop of tubing, then the valve was switched so that the sample entered the tubing leading to the column. The volume of sample could be varied by changing the length of the tubing which held the sample prior to injection. In normal data runs, 0.5 ml. of sample was used.

The column was a Chromatronix model LC-1 one-inch diameter glass column equipped with a water jacket. The volume of the column could be varied between about 270 and 190 ml. by moving the bed supports. The bed supports also acted as flow spreaders for the entrance and exit streams. The efficiency of these flow spreaders was checked often during data runs with a colored solute, and they were evaluated in an extra column study which will be discussed later. The temperature of the column was maintained by a recirculating water bath connected to the water jacket. The temperature was measured by a thermometer fastened inside the water jacket, and the variation was estimated at $\pm$ 0.05°C.

Solute concentration in the effluent was continuously measured with a modified Nester/Faust Model 404 RI monitor and recorded by a Sargent model S-72150 millivolt recorder. The RI monitor was first modified by adding an optional shunt circuit to the inductance-capacitance damping network. The second modification was to pack the flow channels in the optical head with 200-μm. glass

beads. The packing was necessitated after observing exaggerated tailing of elution curves which were obtained when a small volume of sugar solution was injected directly into the detector. After this modification, nearly symmetrical curves were obtained. The optical head was isolated inside a section of plastic conduit inside a constant temperature bath; estimated temperature variation was $\pm$ 0.005°C.

The detector was calibrated both statically and dynamically with flowing sugar solutions, and it was found that there was no difference between static and dynamic sensitivities. Depending on the temperature of the water bath, the sensitivity was between 5 and 10 mv. $g.^{-1}$ (100 ml.), i.e., 5 to 10 mv. $percent^{-1}$. The millivolt output was in all cases proportional to the sugar concentration (percent, w/v). The sensitivity was the same for dextran, glucose, sucrose, and raffinose.

COLUMN PACKING TECHNIQUE

The column was repacked many times during the course of the work, and the following is an account of the procedure which was found to work best with gel materials. No completely satisfactory technique was established for packing columns with glass beads. The first criterion used to assess a packing technique was if the deposited gel was formed as a layer perpendicular to the column axis. The second criterion was the behavior of the colored solute band as it was injected and moved down the column. The third criterion was the symmetry of the colored band as it was recorded by the RI monitor. On certain rare occasions, it was found that the curve was nearly symmetrical; and from this it was inferred that some of the dissymmetry might be attributed to poor packing.

The column was washed and dried in an oven at 110°C., cooled, and filled with a 5% solution of dichlorodimethylsilane in benzene. After about an hour, the solution was removed, and the column was heated to 110°C. for an hour. This treatment was to eliminate any solute adsorption on the column; it was repeated periodically during the work.

Before packing, the column was dried and aligned vertically with a plumb bob or a carpenter's level. The bottom bed support was inserted, and the column was filled with water by a siphon inserted to the bottom of the column. After the water had reached the regulated temperature, a deaerated gel slurry was poured into a large funnel fastened to the top of the column. No stirring was necessary to keep the gel from plugging the funnel. After a layer of about 3 cm. had deposited, the effluent tube was opened, and the water was removed at a moderate rate, about 3 ml./min.

After all the gel was packed, the effluent line was closed and the entrance port was inserted above the packing. The packing was conditioned by pumping water through the column at a high flow rate until no further reduction was found in the packed length. The entrance support was lowered to the surface of the gel, the packing was tested with colored solute, and the system was ready for a data run. The packing was stable except when pulsing flow or upward elution were used. The packing was not disturbed during normal data runs.

EXPERIMENTAL PARAMETERS

PARTICLE DIAMETER MEASUREMENTS

Samples from each of the three Bio-Gel P-2 fractions were characterized by measuring the diameters of approximately 1500 particles. Three slides were made from each of the fractions and about 500 particles were measured from each of the slides. The G-10 and G-15 gels were characterized by about 1000 measurements on each sample. About 500 diameters were measured from the glass bead samples.

Gel fractions were sampled by the method described by Isenberg (49) for wood fibers. A drop of dilute slurry was placed on a microscope slide and the particles were stained with a 0.5% aqueous solution of methylene violet. The particles remained in a water slurry during the time of measurement.

Measurement of particle diameters was done with the digital coding micro-comparator. This device projects a magnified image from a movable stage onto a ruled screen. The X-Y position of the stage is coded to digital information and this may be recorded on data cards as increments of 2.1167 μm. (50). In practice, the image of a particle was brought tangent to a grid line and this coordinate was recorded; then the opposite side of the particle was brought tangent and the second coordinate was recorded. Computer programs were written to compile the sets of diameter data and to reduce them to a useful form. Appendix III gives a listing of the particle analyses which apply to this work.

A single particle was measured 52 times in order to ascertain the error associated with particle measurement. The measurements were made rapidly, as in the measurement of a distributed gel sample. The measurements of a single particle have a standard deviation of 2.53 μm. This error is comparable to the precision of the instrument, viz. 2.12 μm.

The changes in gel size with temperature were analyzed in the following way. The packing porosity at each temperature can be written as

$$\varepsilon_T = \frac{V_{o,T}}{V_{t,T}} = \frac{V_{o,T}}{V_{o,T} + V_{g,T}} \tag{23}$$

where

$V_{o,T}$ = void volume at temperature T, cm.^{3}

$V_{t,T}$ = total volume at temperature T, cm.^{3}

$V_{g,T}$ = volume occupied by swollen gel at temperature T, cm.^{3}

ε_T = column porosity at temperature T, dimensionless.

In all data runs with a given gel fraction, the same quantity of gel was used. It was quantitatively removed and repacked into the column. The number of particles in each gel fraction can be calculated from the equation

$$N_p = \frac{V_{g,30}}{\pi/6\ d^3} \tag{24a}$$

where

N_p = number of particles

d = spherical volume average particle diameter as defined in Equation (35)

$V_{g,30}$ = calculated gel volume at 30°C.

Taylor's theorem was used to derive an expression for the small change of d with V_g. The result was the following equation:

$$\Delta d \approx \frac{\Delta V_g}{3\ V_{g,30}^{2/3}} \left\{ \frac{6}{\pi\ N_p} \right\}^{1/3} \tag{24b}$$

where

$\Delta \underline{d}$ = change of particle diameter with temperature compared to $\underline{d}$ at 30°C.

$\Delta V_{\underline{g}}$ = change in calculated gel volume with temperature compared to 30°C.

The results of analyzing the data for the three Bio-Gel P-2 fractions are given in Table IV. The only change which was significant occurred at 15°C. with the 50-60 mesh fraction; this correction was made for the data run at this temperature. The major source of error in this analysis was probably in the measurements of void volume.

TABLE IV

VARIATION OF GEL DIAMETER WITH TEMPERATURE

Fraction	Temperature, °C.	$\Delta \underline{d}$, μm.
50-60 mesh	15	-3.57
	45	-0.32
70-80 mesh	15	-0.27
	45	-0.13
100-120 mesh	15	-0.12
	45	-0.04

EXPERIMENTAL VARIABLES

ELUTION VOLUME, $V_{\underline{e}}$

The elution volumes of solutes were initially measured as the volume that passed through the column between injection and peak detection. This volume was corrected for the dead volumes in the system to give the true elution volume, peak entrance to peak exit. The volumes were calculated from a measured distance on the recorder chart using the chart speed and the volumetric flow rate of the eluant. During a data set, the measured elution volume of a solute varied over a range of about $\pm$ 2.5 ml. or about 2% of the mean elution volume. The main source of error

was the inability to maintain a precise flow rate. A secondary source of error was the volume changes in the system caused by wide variations in the room temperature.

VOID VOLUME, $\underline{V}_o$

The column's void volume was measured as the elution volume of the non-partitioned solute, Sephadex Dextran 10. Solutions of 1.0 to 2.5% dextran were injected and recorded at each flow rate in a data set. This gave several measures of $\underline{V}_o$ and also gave data on the spreading behavior of this solute.

TOTAL VOLUME, $\underline{V}_t$

The total volume of the column was measured as the product of the cross-sectional area and the packed length. The manufacturer's specifications were used for the area and a cathetometer was used to measure the packed length.

VOLUMETRIC FLOW RATE, $\underline{Q}$

The volumetric flow rate was measured by weighing the effluent for ten or twenty minutes. Dividing the mass flow rate by the density, unity, gave a measurement of the flow rate to $\pm$ 0.001 ml./min. The flow rate was the most difficult parameter to control due to the nature of the eluant pump. The flow rate was adjusted to an approximate value using a flowmeter, then it was measured periodically during the data run. The maximum variation was about 2% over an elution volume of around 150 ml. An average was calculated for each solute so that the flow rate was representative of the period between injection and peak detection.

DERIVED QUANTITIES

HEIGHT EQUIVALENT OF A THEORETICAL PLATE, HETP

The parameter HETP was used as the dependent variable describing band spreading in the various GPC systems investigated. This quantity may not be the most fundamental measure of band spreading; however, it is the one most commonly used and understood by workers in the field of chromatography. The physical meaning of HETP was discussed previously (p. 15), and two examples were given to illustrate the relationships of variables. The experimental measurement of HETP is based on the premise that the elution curves are in the shape of normal curves of error.

The experimental elution curves were all close approximations to the shape of a normal curve. As illustrated in Fig. 9, the symmetry of each curve was tabulated as the ratio of the two half widths. For partitioned solutes, the width ratio ranged from about 1.6 to 0.9 with the mean at 1.1. Dextran curves were more skewed with a range from 0.8 to 2.0 and the mean at about 1.3. It is difficult to account for the dissymmetry except in a qualitative way.

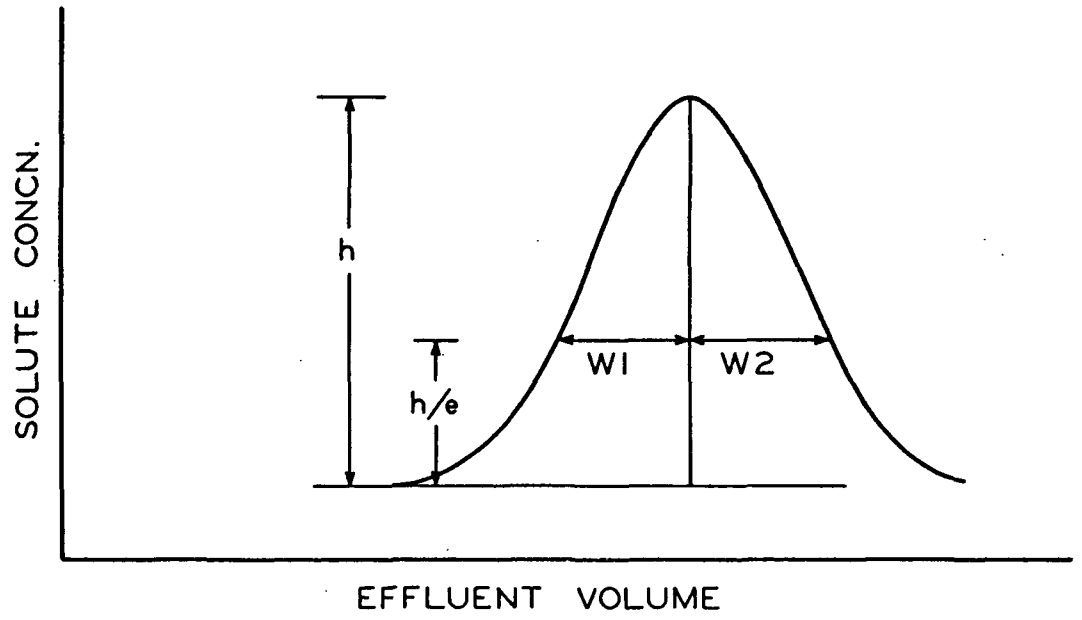

Figure 9. Elution Curve Width Measurements

The response of the RI monitor probably lagged behind the actual solute concentration in the effluent. This lag was reflected in the measurements of the extra column curves. The measured area under these curves was about 1.01 times larger than the theoretical area, and the width ratio of the extra column curves was about 1.6.

The equations for calculating HETP have been critically reviewed by Purnell (20). All of the equations are equivalent when: (a) the elution curves are exactly normal, and (b) there are a large number (about 3000) of theoretical plates. The equation used in this work was derived by Glueckauf (24).

$$N = 8 \frac{V_e (V_e - W1)}{(W1 + W2)^2} \quad . \tag{25}$$

This equation gives the correct number of theoretical plates at low values of N and is the least sensitive of all curve measurements to skewness (20).

Due to the special condition at the column entrance, the measured length of packing was corrected for the finite feed volume (14).

$$L' = L - \chi \quad . \tag{26}$$

where

L' = corrected column length, cm.

L = measured column length, cm.

$\chi = V_f / 2A\varepsilon$ = about 0.13 cm. for a typical experiment.

The experimental value of HETP was measured according to the equation

$$H = L'/N \quad . \tag{27}$$

An example of curve measurement is given in Appendix II along with the working equations which were used in compiling the data.

MASS TRANSFER PARAMETERS, D_g and K_L

As described in Appendix II, a computer program was written to calculate H, α, and U from each of the curve measurements. Included in the program was a section which calculated the best slope, m, from the experimental $H\alpha$ vs. U data. The least-squares deviations method was used in the calculations.

From the slope m and the experimental volumetric parameters, the mass transfer variables were calculated through the following equations:

$$D_g = \frac{F1\ d_p^2}{30\ m}, \tag{28}$$

$$1/K_L = m/2\ F2, \tag{29}$$

$$F1 = \frac{V_o\ (V_e - V_o)}{V_e^2}, \tag{30}$$

$$F2 = \frac{V_o}{V_t}\left(\frac{V_e - V_o}{V_e}\right)^2. \tag{31}$$

SOLUTE SOLUTION PROPERTIES

Literature sources were used for the diffusion coefficients listed in Table V.

The temperature dependence of the diffusion coefficients was calculated by the Stokes-Einstein equation using the viscosity of water (41).

TABLE V

DIFFUSION COEFFICIENTS

Solute	D_m, 25°, cm.^{2} sec.$^{-1}$	Source
Glycine	10.64×10^{-6}	(44)
Glycerin	9.4×10^{-6}	(51)
Glucose	6.73×10^{-6}	(44)
Sucrose	5.21×10^{-6}	(44)
Raffinose	4.34×10^{-6}	(44)
Schardinger alpha-dextrin	3.44×10^{-6}	(52)
Schardinger beta-dextrin	3.22×10^{-6}	(52)
Sephadex Dextran 10	1.095×10^{-6}	(53)

EXTRA COLUMN CORRECTIONS

The auxiliary equipment in a chromatographic system is responsible for band spreading that is separate from that which occurs in the chromatographic column. In order to evaluate this additional dispersion, the support assemblies from the chromatographic column were inserted into a short brass column and held directly against each other. This false column was used in place of the chromatographic column. The other components shown in Fig. 8 remained the same. Sugar solutions were injected into this system and the elution curves were measured as discussed in Appendix II. The data were compiled by a separate computer program which calculated an elution volume correction and a spreading correction.

In normal data runs, the elution volume was measured as the volume between injection and peak detection. The value which must be used for theoretical analysis is the volume between peak entrance and peak exit from the column. The difference between these values is due to the dead volumes associated with the auxiliary components. The correction volume was determined to be 3.17 ml. for a 0.5 ml. initial feed volume. (This was the feed volume that was used in all data runs.) The standard error was found to be 1.1%, and there was found to be no variation with flow rate or solute concentration.

The apparent spreading due to auxiliary sources was evaluated according to a method suggested by Aris (54) based on the additivity of variances for flow vessels in series. The HETP correction was determined by injecting a sample into the system and measuring the variance of the resulting elution curve. The equation used to calculate the correction was

$$HCOR = \frac{L\,W^2}{8\,V_e^2} \quad , \tag{32}$$

where

HCOR = HETP correction to be subtracted from the normal elution calculation, cm.

L = length of column, cm.

V_e = elution volume of normal solute, $cm.^3$

W = width of extra column at height/e (e = 2.71....), $cm.^3$.

It was found that the HETP correction was independent of both flow rate and sample concentration, standard error 3.5%. There was no variation with sample volume up to 1.5 ml. The magnitude of the correction depends on the elution volume of the solute to which it is applied as indicated in Equation (32). Under conditions characteristic of this work, the correction was about 0.00045 cm. The overall HETP ranged from 0.04 to 0.8 cm., making the correction always less than 1%. Since the correction was so small, it was neglected when treating the experimental results.

RESULTS AND DISCUSSION

ANALYSIS OF THEORY

The data used to examine the theory consisted of measurements taken at three temperatures (15, 30, and 45°C.) for three diameter fractions of Bio-Gel P-2 using two partitioned solutes (glucose and raffinose). The data were reduced to the slopes and intercepts of the plots of $\underline{H\alpha}$ vs. $\underline{U}$ as previously discussed. These data were used to calculate the quantities $\underline{H_o}$, $\underline{K_L}$, and $\underline{D_g}$, and these parameters formed the basis for examining the theory.

CHOICE OF DIAMETER AVERAGE

Many equations exist for calculating an "average" particle diameter (55). Equations (10) and (18) require a measurement of the gel particle diameter which corresponds to the process of mass transfer. A search of the literature gave scant information regarding the proper average. The most advanced theoretical studies (54, 56) gave an average which reduced to the surface average diameter after simplification, Equation (36). There were no experimental studies dealing with the choice of an appropriate average. Therefore, the following analysis was made.

The following equations are the averaging methods which were used:

$$d_{sps} = N \left(\frac{N}{\Sigma 1/d} \right)^{-1} = \text{specific surface average diameter} \qquad (33)$$

$$d_n = \frac{\Sigma d}{N} = \text{number average diameter} \qquad (34)$$

$$d_{sv} = \left(\frac{\Sigma d^3}{N} \right)^{1/3} = \text{spherical volume average diameter} \qquad (35)$$

$$d_a = \frac{\Sigma d^3}{\Sigma d^2} = \text{area average diameter} \qquad (36)$$

$$d_{wv} = \frac{\Sigma d^4}{\Sigma d^3} = \text{weight or volume average diameter} . \qquad (37)$$

Equations (34), (36), and (37) give the averages which are commonly measured by microscopic analysis, by light scattering, and by standard screen analysis, respectively. The naming of these averages is consistent with practice (55). Equations (33) and (35) calculate a diameter which is equivalent to the most probable specific surface and spherical volume, respectively. These averages have not been discussed in literature dealing with small particle statistics. Figure 10 is a schematic presentation of the averages for the three fractionated Bio-Gel P-2 gel samples. See Appendix III for a catalogue of the data.

A simplified method of comparing relative deviations was used to ascertain the error associated with each average. The starting point was to assume that Equations (10) and (18) were exact. Using each of the diameter averages, the values of $\underline{D}_g$ and $\underline{K}_L$ were calculated for the solutes in each data run.

Since the actual values of $\underline{D}_g$ could not be obtained, the analysis was done by calculating and combining the average deviations of $\underline{D}_g$ from group averages. The first group was constant temperature, same solute, between gel fractions. The analysis was extended to groups between temperatures, then between solutes. Differences between group means were considered, and the deviations were normalized before combination. Appendix V gives a more detailed description of the analysis method. The normalized relative deviations from this study are shown in Fig. 11, abbreviated $\Delta\underline{D}_g$.

The overall mass transfer coefficient is related to the "average" gel diameter by the equation

$$\log 1/K_L = 2 \log d_p - \text{constant}$$

which predicts a slope of 2 for the log-log plot of $1/\underline{K}_L$ vs. $\underline{d}_p$. The slopes were calculated by regression analysis for each of the diameter averages. The deviations

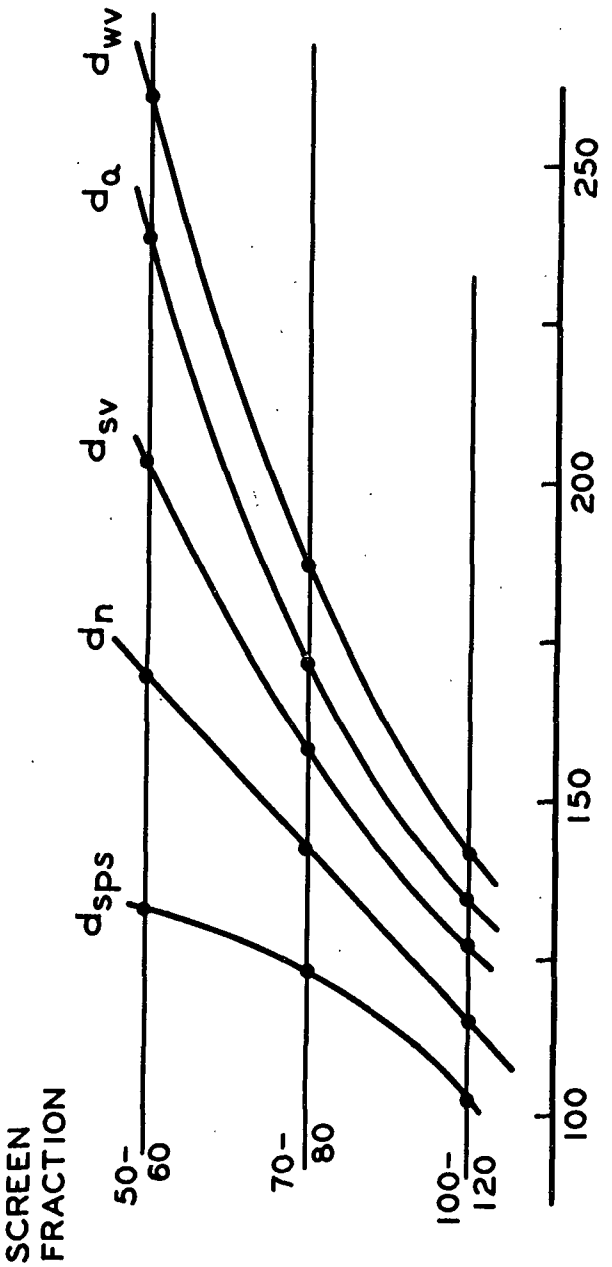

Figure 10. Average Diameters for Fractionated Gel

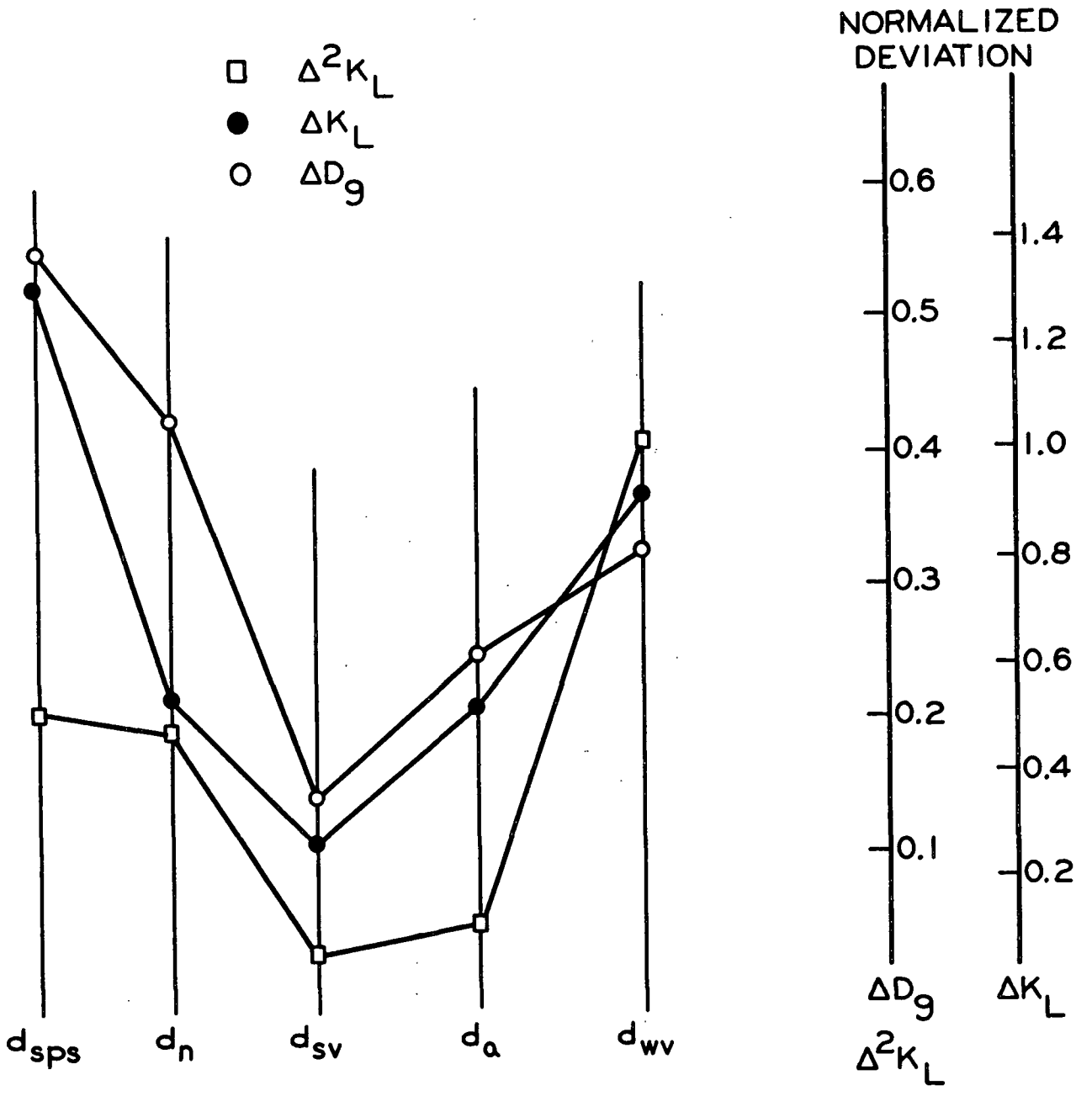

Figure 11. Error Analysis of Diameter Averages

of the slopes from the value 2.00 were compiled, and this error is shown in Fig. 11, abbreviated ΔK_L.

Regardless of the exponent of d_p, it should be the same for both solutes, glucose and raffinose. This is to say that the mass transfer mechanism is equivalent for the two solutes. This analysis was made and the error is shown in Fig. 11, abbreviated $\Delta^2 K_L$.

Figure 11 shows that a minimum error occurs for the spherical volume average with each of the three measurements. This is not an unreasonable result since slow particle diffusion is a volume-dependent mechanism. The spherical volume diameter average was used in the following analysis of theory.

REPRODUCIBILITY

In studies of porous beds, the consistent formation of uniform packing is an important experimental consideration. In order to assess the experimental variations, the conditions at 45°C. with the 50-60 mesh gel were repeated four times. The column was repacked between each of the runs. The slopes and intercepts from this study are compared in Table VI.

The large amount of variation in H_o reflects the changes in pore structure between formations of the packing. This makes it difficult to compare the effects of axial dispersion between repacked columns. As shown in Table VI, there was only nominal variation in the slopes and distribution coefficients. This indicates that the mass transfer parameters can be compared between repacked columns.

TABLE VI

REPRODUCIBILITY DATA

	Raffinose			Glucose			
Run	$\underline{m}$	$\underline{H}_o$	$\underline{K}_1$	$\underline{m}$	$\underline{H}_o$	$\underline{K}_1$	ε
13	11.50	0.079	0.291	4.34	0.068	0.412	0.354
46	11.71	0.040	0.296	5.03	0.029	0.414	0.365
47	11.76	0.052	0.288	4.89	0.044	0.414	0.381
48	11.33	0.041	0.293	4.93	0.034	0.412	0.368
Mean	11.58	0.053	0.292	4.80	0.044	0.413	0.367
Av. dev.	0.16	0.013	0.005	0.23	0.012	0.001	0.007
Dev., %	1.4	25	1.7	4.8	27	0.24	1.9

Average correlation coefficient = 0.993

$\underline{m}$ = slope of $\underline{H}\,\alpha$ vs. $\underline{U}$, sec.$^{-1}$

$\underline{H}_o$ = intercept of $\underline{H}\,\alpha$ vs. $\underline{U}$, cm.

"Run" specification refers to pages in I.P.C. Research Notebook No. 2607.

AXIAL DISPERSION

There was no indication of longitudinal diffusion even at the slowest flow rates used in the study, ca. 0.2 ml./min. The effects of longitudinal diffusion would have been indicated by a rapidly increasing $\underline{H}$ with decreasing $\underline{U}$ at low flow rates. All of the experimental plots of $\underline{H}$ or $\underline{H}\,\alpha$ vs. $\underline{U}$ were linear.

In the absence of longitudinal diffusion, the extrapolated value of $\underline{H}\,\alpha$ at $\underline{U} = 0$ is the measurement of "eddy diffusion." As suggested by Golay (57), a more descriptive term for this effect would be "multipath" dispersion; however, this term has not been used in the literature. The more general term "axial" dispersion will be used to refer to this effect.

There is short-range variability in the fluid speeds throughout the column packing. A fluid element following a streamline is forced to change its velocity continuously because the available cross section along its path is nonuniform. In

a period of time, a molecule following a streamline will travel a different distance down the column, compared to a molecule in another streamline. These contributions of axial dispersion to band spreading were first described by the theories of random walk (20). Under normal conditions of GPC operation where $\underline{U} > 2\ \underline{D_m}/\underline{d_p}$, the axial contribution is given by (14)

$$H_e = 2\ \lambda\ d_p \qquad (38)$$

where

$$\lambda > 0.5.$$

At very low flow rates, there is a velocity dependent term which accounts for solute diffusion across streamlines.

In the derivation discussed in a previous section, the axial dispersion term was given as

$$H\ \alpha = 2\ \lambda\ d_p \quad . \qquad (39)$$

Noting that when $\underline{U} \rightarrow 0$, $\underline{H} \rightarrow 0$, and $\alpha \rightarrow 1$, the intercept can be written as

$$H_o = 2\ \lambda\ d_p \quad . \qquad (40)$$

Considering the statistical treatments of axial dispersion (26), the most consistent diameter to use with Equation (40) would be either the number (N) or the specific surface (SPS) average. As shown in Fig. 12, there is a linear dependence of dispersion on both of the averages, except for the 70-80 mesh data. Special precautions were taken during these data runs, so it is not unreasonable that there is no agreement.

The slopes of the lines in Fig. 12 are one measure of λ as can be seen from writing Equation (40) in the form $\underline{H_o}/2 = \lambda\ \underline{d_p}$. These slopes are compared to the simple average $\langle\lambda\rangle$ from normal data reduction in Table VII.

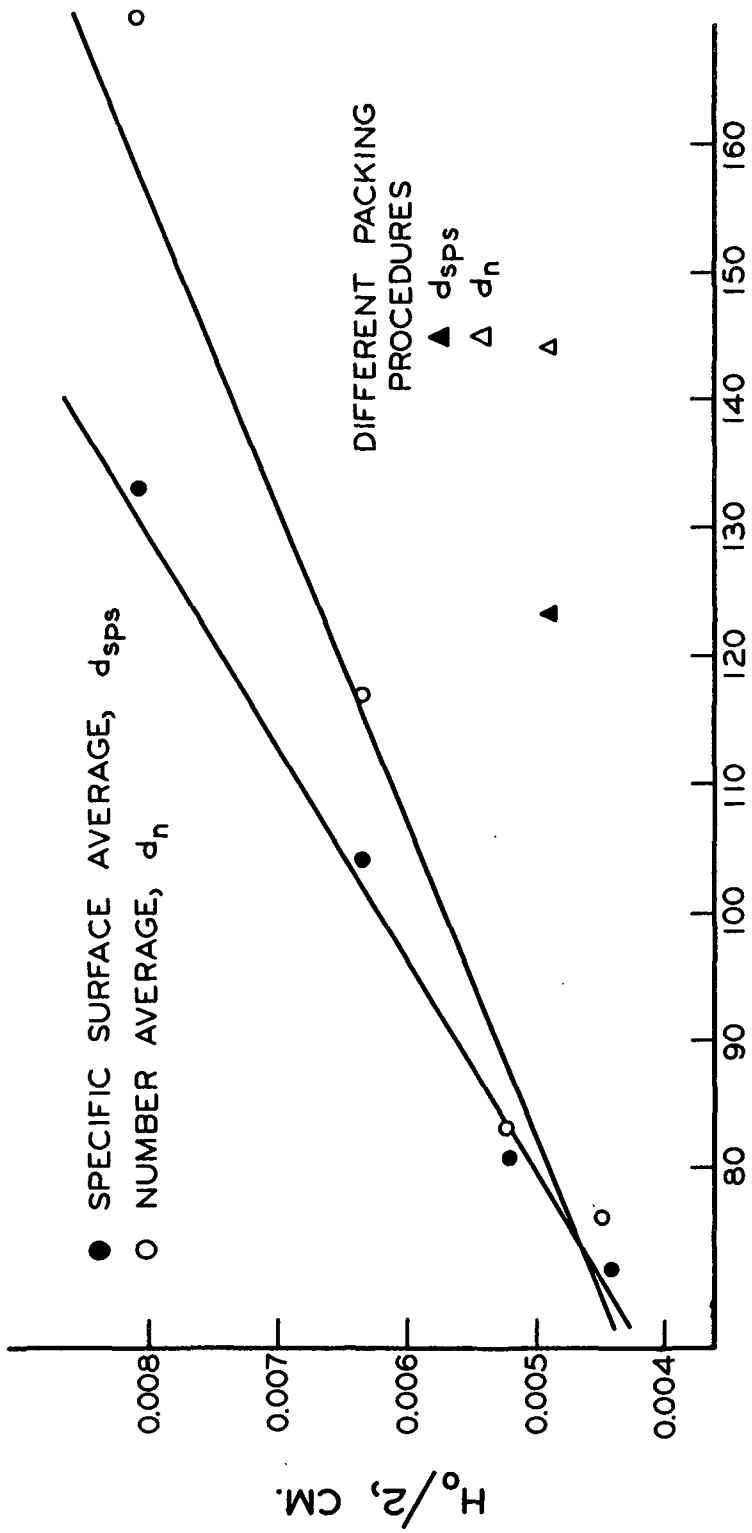

Figure 12. Axial Dispersion Dependence on Average Particle Diameter

TABLE VII

DEPENDENCE OF AXIAL DISPERSION ON PARTICLE DIAMETER

	$\underline{d}_{SPS}$ Basis	$\underline{d}_{n}$ Basis
Correlation Coefficient[a]	0.998	0.991
Intercept[a]	3.5×10^{-4}	1.9×10^{-3}
Slope[a]	0.583	0.368
$\langle\lambda\rangle$	0.620	0.557
$\langle\lambda\rangle$ − Slope	0.037	0.189

[a]Refers to data shown in Fig. 12.

The correlation coefficient is larger and the intercept is smaller for the SPS average. Intuitively, this indicates closer description of the real system with the SPS average. There is a better agreement between $\langle\lambda\rangle$ and slope for SPS than for N basis. From these comparisons, the conclusion is that the SPS average gives the most consistent measure of particle diameter with reference to the random walk theory of axial dispersion.

MASS TRANSFER

As discussed previously, there are several sources of resistance to mass transfer in an operating GPC column. In analyzing the theory, the first question is whether or not slow gel phase transport was the predominant mass transfer retarding mechanism. The second question is whether or not the derivation leading to Equation (18) is sufficient for the description of band spreading in GPC.

The overall mass transfer coefficient can be written in the form

$$\ln 1/K_L = 2 \ln d_{sv} - \ln 60 \hat{D}_g K_1 \qquad (41)$$

where $\hat{D}_g$ is to be distinguished from D_g which is given by

$$D_g = \frac{Fl\ d_{sv}^2}{30\ m} \quad . \tag{42}$$

As can be seen from Equation (41), the log-log plot of $1/K_L$ vs. d_{sv} should be linear with a slope of 2 and an intercept of $-\ln 60\ \hat{D}_g\ K_1$. The data were reduced by regression analysis and the results are shown in Table VIII.

TABLE VIII

K_L ANALYSIS

Condition	Slope	Intercept	Correlation Coefficient
15°, Glucose	2.18	12.6	0.999
30°, Glucose	1.92	11.0	0.984
45°, Glucose	1.86	10.4	0.984
15°, Raffinose	1.77	12.3	0.989
30°, Raffinose	1.95	12.5	0.992
45°, Raffinose	1.85	11.6	0.999

The linearity of the data indicates that there is not a change in mass transfer mechanisms with changing particle size – at least over the range which the data cover. The slope is the most sensitive test of the mechanism. Slow film diffusion is the only other important mechanism, and theories dealing with this predict a slope of 1.0 or less (16, 23). As can be seen in Table VIII, all of the experimental slopes were very close to 2.0. Using the intercepts to calculate $\hat{D}_g$ gave values which were off by about 30%. However, this is not a sensitive test since the data had to be extrapolated over a long numerical range. The conclusion from this analysis is that slow gel phase mass transport was responsible for the velocity dependent band spreading.

The gel phase diffusion coefficient should be constant between gel fractions at the same temperature. These data are compared in Table IX for the three diameter fractions of Bio-Gel P-2. Considering the many sources of experimental error, there is good agreement between these coefficients.

TABLE IX

$\underline{D}_g$ ANALYSIS

Temperature, °C.	Glucose, $\underline{D}_g \times 10^7$			Raffinose, $\underline{D}_g \times 10^7$		
	100-120	70-80	50-60	100-120	70-80	50-60
15	3.13	3.02	2.85	1.00	1.04	1.01
30	4.82	5.25	3.73	1.72	1.79	1.14
45	6.40	7.84	7.03	3.02	2.85	2.97

Using Eyring's absolute rate theory (58), the gel phase activation energy of diffusion can be calculated from the equation

$$\ln D_g = - E_a (1/RT) + \text{constant} . \qquad (43)$$

The activation energies between gel fractions should be constant; this test is shown in Table X. The agreement is good except for the 100-120 mesh gel fraction. There was more uncertainty in these data sets because of the low sensitivity of band spreading to fluid velocity. This resulted in numerically small slopes in the $\underline{H}\,\alpha$ vs. $\underline{U}$ plots. Consequently, these data runs were more sensitive to experimental variations.

TABLE X

E_a ANALYSIS, BETWEEN GELS

	E_a, kcal./mole		
	50-60	70-80	100-120
Glucose	5.55	5.54	4.45
Raffinose	6.14	6.12	7.34

The physical meaning of the activation energies is difficult to assess in the aqueous gel systems. The gel and the solutes are hydrogen-bonding materials and this effect is temperature sensitive. In diffusion through gels there is a decrease in diffusivity due to solute-gel interaction. This effect would also be temperature sensitive since there is increasing segmental diffusion of the gel with increasing temperature (44).

Intuitively, one would expect an increasing activation energy with increasing solute molecular weight and with decreasing gel porosity. The data of Spacek and Kubin on KCl.-glycolmethacrylate systems (42) indicate that the activation energy does decrease with increasing porosity – to a value close to diffusion in water. Horowitz and Fenichel used tracer methods to measure diffusion of neutral solutes in a dextran gel, Sephadex G-34 (59). Their data show a slight increase in activation energies with molecular weight. This Sephadex G-34 study and the Bio-Gel P-2 study of this thesis are not exactly comparable since P-2 is more highly cross-linked, and the solutes used with P-2 gel were of larger molecular weights. The experimental activation energies of gel phase diffusion are shown in Table XI for the solutes studied in this work. The energies increase in the expected order and they are close to the values obtained from independent methods, cf. 4.5-5.9 kcal./mole (59) and about 6.0 kcal./mole (42).

TABLE XI

E_a ANALYSIS, BETWEEN SOLUTES

Solute	E_a, kcal./mole
Glucose	5.34
Sucrose	5.90
Raffinose	6.50
Schardinger alpha-dextrin	6.53
Schardinger beta-dextrin	6.73

In summary, the analysis of the experimental measurements has indicated that slow gel phase diffusion controls transport resistance. Furthermore, the linear flux equations are sufficient to describe the dynamic spreading behavior. The experimental observations were consistent with the theory and with the qualitative understanding of the process. There was good agreement with the limited number of independent studies of related gel phase diffusion.

INTERPRETATION OF RESULTS

The following sections deal with experimental results which have no direct bearing on the theory of band spreading. These results are discussed with the intention of improving the qualitative understanding of GPC. The interpretation will be based in part on the theory developed in this thesis and in part on the work of others.

MISCELLANEOUS FACTORS

Some of the operating parameters were qualitatively examined using Bio-Gel P-2, 70-80 mesh preparation. An effort was made to control the flow rate at 1.5 ml./min., but this was not possible. The data were normalized to 1.5 ml./min. using the experimental results from normal data runs.

In all cases, distribution coefficients of the solutes were found to be constant within experimental error. There was no variation between temperatures, gel fractions, or packing porosities. There was no variation with flow rate.

The amplitude of pumping pulsations was studied by changing the tubing arrangement on the Sigma pump. A single 1/4 inch outside diameter Tygon tube gave high pulsation – similar to an unmodified single-piston pump. Nearly steady flow was obtained with a duplex manifold of 1/16 inch outside diameter tubing. (This is the arrangement which was used in normal data runs.) An intermediate amplitude was obtained with a single 1/8-inch outside diameter tube. As shown in Fig. 13, the level of pulsation had no significant effect on band spreading. High-amplitude pulsations did have the effect of destabilizing the column packing, causing the packing to compress during elution.

There was no effect of sample volume on HETP as shown in Fig. 14. This is the usual observation until a certain limit is reached, beyond which there is a rapid increase in HETP with sample volume (60).

Increasing the dextran concentration led to fingering above the approximate limit of 3.5% (w/v). As discussed previously, the phenomenon of fingering is due to instabilities at the fluid boundaries of the solute zone. It was found that the observed band spreading could be reproduced with a given packing, but the effect was variable between packings. As shown in Fig. 15, HETP was essentially constant up to about 3.5% and then increased rapidly as fingering became more pronounced. The elution curves of the concentrated bands were distinctly different from the curves recorded with dilute dextran solutions. There were secondary inflections, making the appearance similar to the behavior of overlapped bands.

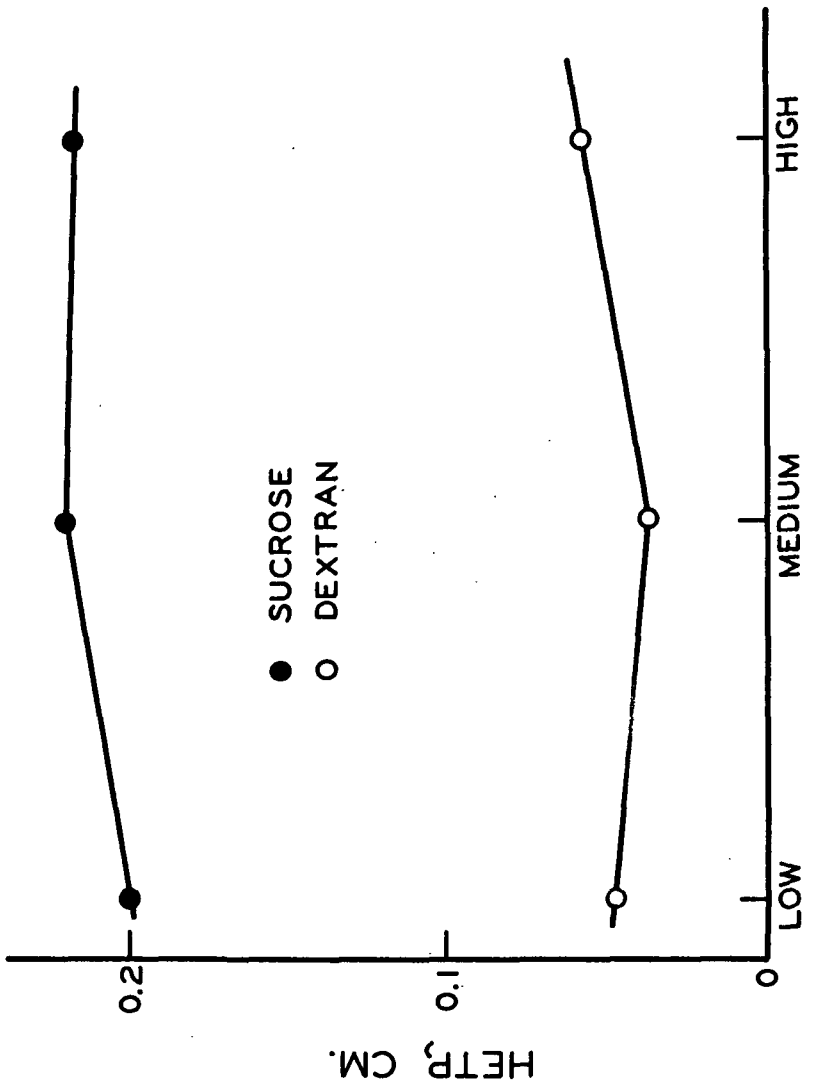

Figure 13. Effect of Pumping Pulsations, 15°C.

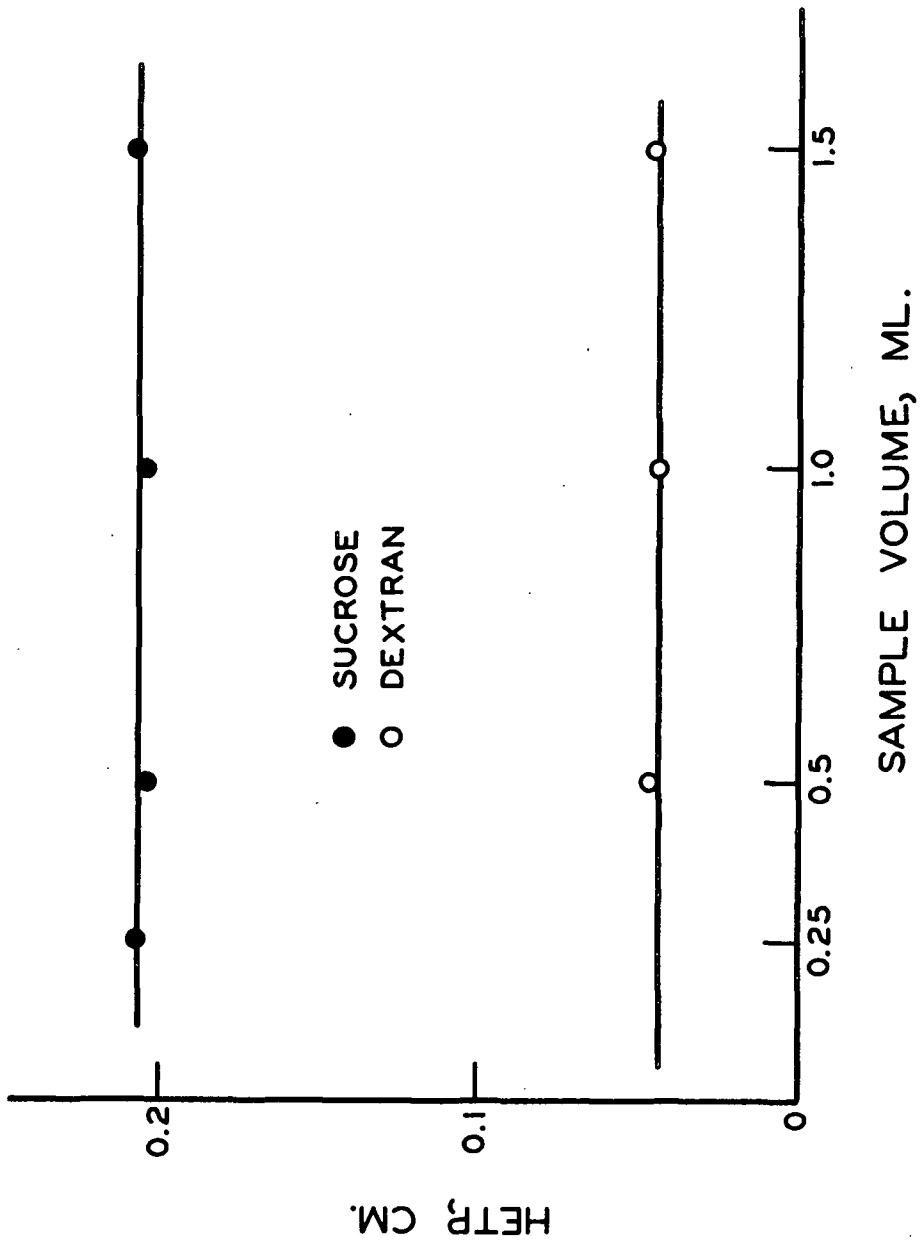

Figure 14. Effect of Sample Volume, 15°C.

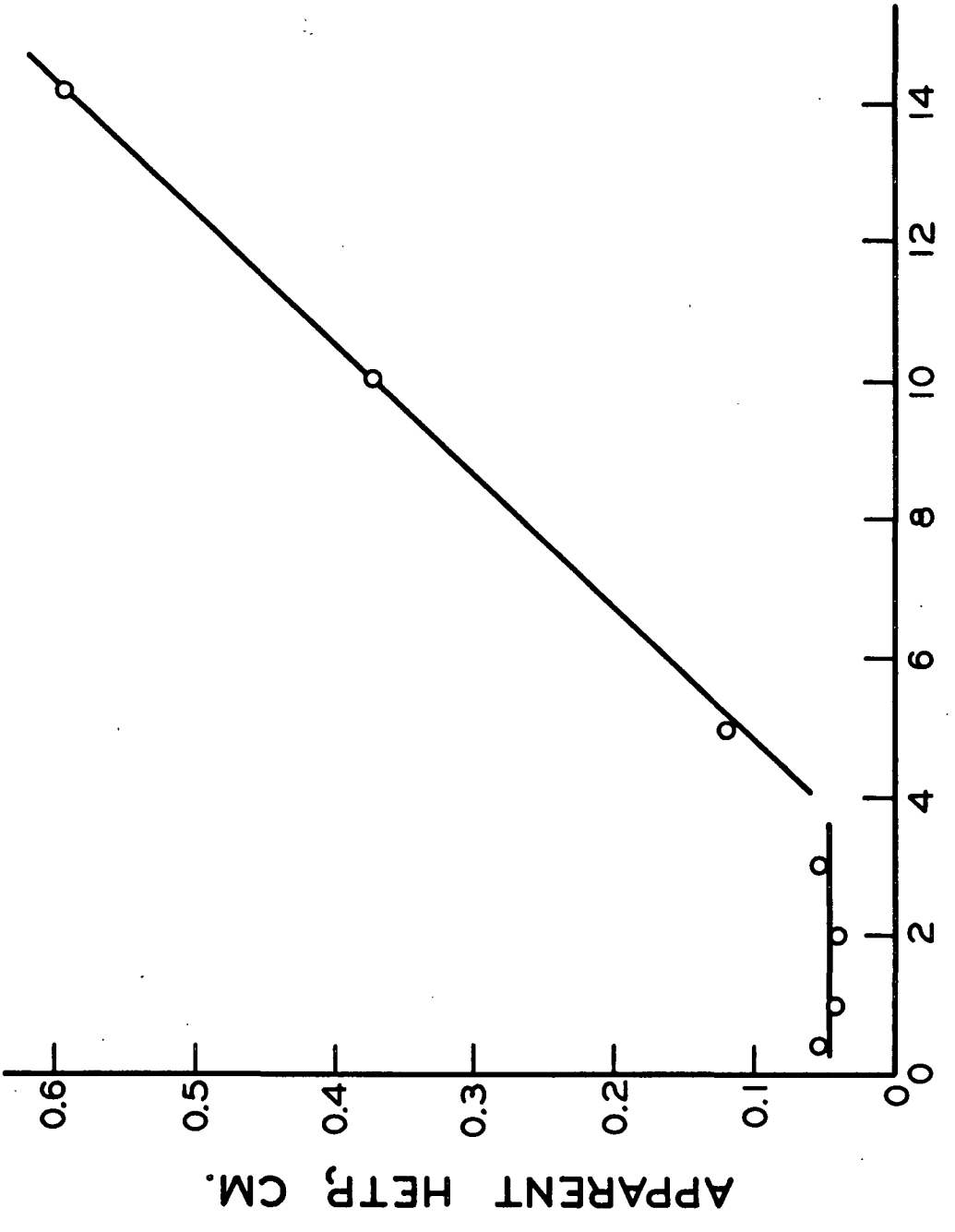

Figure 15. Dextran Fingering, 15°C.

A concentration series was studied with sucrose as the solute. At 15°C., there was no effect up to 20% concentration. At 45°C., the concentration range was extended to 65%, and the results of this study are shown in Table XII. The standard deviation of elution curves was constant up to 20% solutions, then increased with concentration. The increased spreading was accompanied by a change in the curve shape as shown by the area ratios in Table XII. No fingering was observed in the bands of concentrated sucrose samples.

TABLE XII

CONCENTRATED SUCROSE RESULTS

Initial Concentration, %	σ_v, ml.	A_1/A_2 [a]
5-20	7.44 ± 0.15	0.98
35	7.79	1.01
50	8.18	1.04
65	8.54	1.16

[a] A_1 = area under leading half of elution curve, cm.^{2}.
A_2 = area under tailing half of elution curve, cm.^{2}.

AXIAL DISPERSION

Variations in the cross-sectional area of spaces between packed particles is the most obvious cause of axial dispersion. The variations in fluid speeds depend on the pore size distribution as discussed by Sherman (10). This distribution in the GPC systems is a function of packing porosity and of particle size distribution. Another factor, one which is extremely difficult to evaluate, is the variations in bed structure which originate in the column packing procedure.

As discussed in the section on reproducibility, when the column was repacked, there was a large variation between the experimental H_o values. There were a limited number of data runs where the porosity changed and the column was not repacked. This occurred when the temperature was changed, leading to slight volumetric changes in the bulk gel. Figure 16 compares the experimental data taken with and without repacking. As can be seen from this plot there is both a porosity dependence and a particle size effect on axial dispersion. The larger slope of the 133 μm. data indicates a larger sensitivity of axial dispersion on porosity. This would be expected since the pores in these beds cover a larger distribution of sizes.

An effect of flow rate on axial dispersion was observed with 3M Superbrite glass beads. It was difficult to pack the column, and only a limited amount of work could be done with these systems. Figure 17 shows the results of an investigation at two temperatures. At the lower temperature it can be seen that axial dispersion decreases with flow rate, while there is little or no dependence at the higher temperature. At 10°C., the dispersion of the high molecular weight dextran was greater than the dispersion of glucose at all of the flow rates.

Very good axial dispersion data were obtained from dextran solutions in the 70-80 mesh Bio-Gel P-2 runs. Since the column was repacked between runs, the experimental data shown in Fig. 18 has been normalized to give equal intercepts. As seen from this plot the slope decreases with temperature, and a negative slope is obtained at the highest temperature.

The most detailed statistical theory of eddy diffusion (14) reduces to the following equation after simplification:

$$H_o = \frac{2\lambda \cdot d_p}{1 + C/U}, \qquad (44)$$

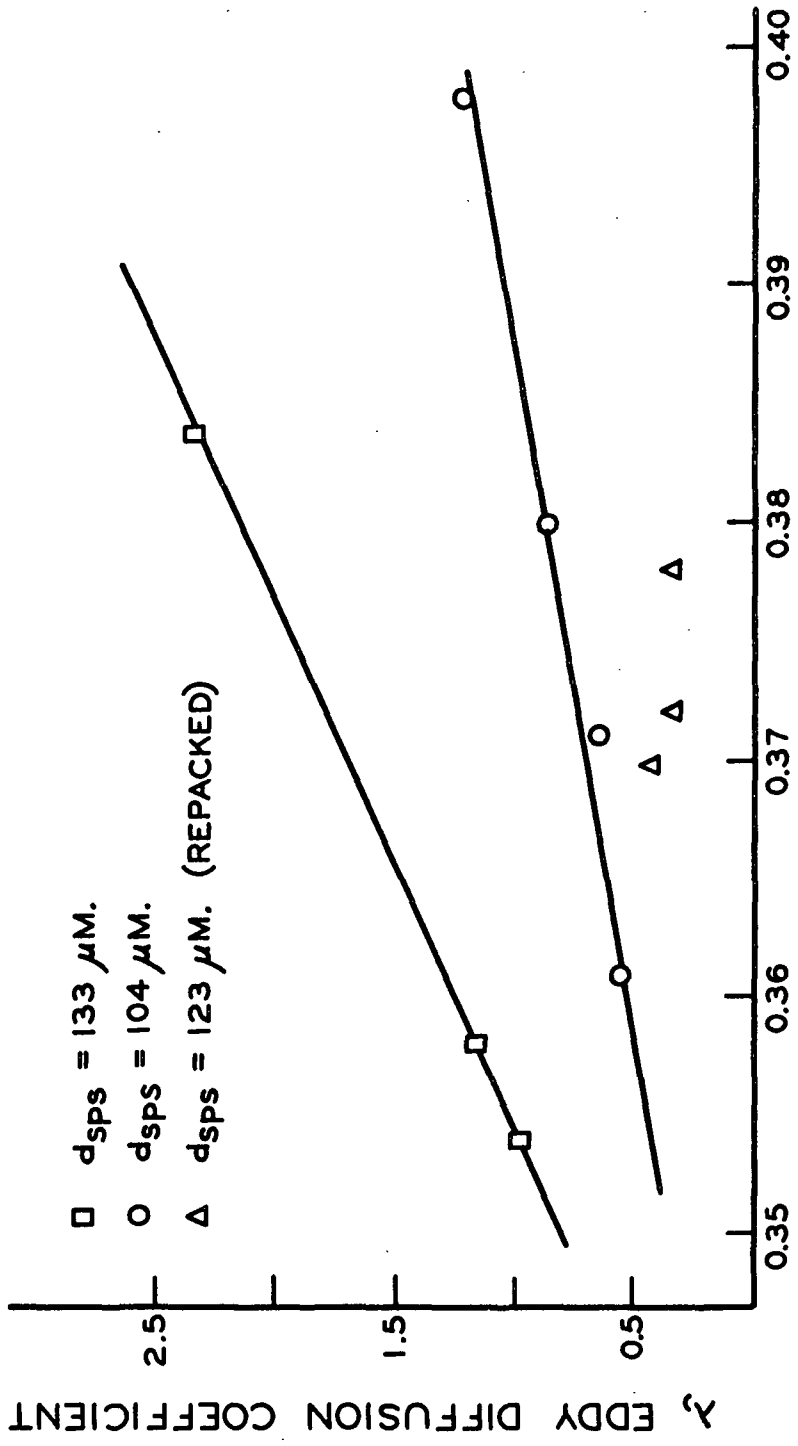

Figure 16. Axial Dispersion as a Function of Packing Porosity

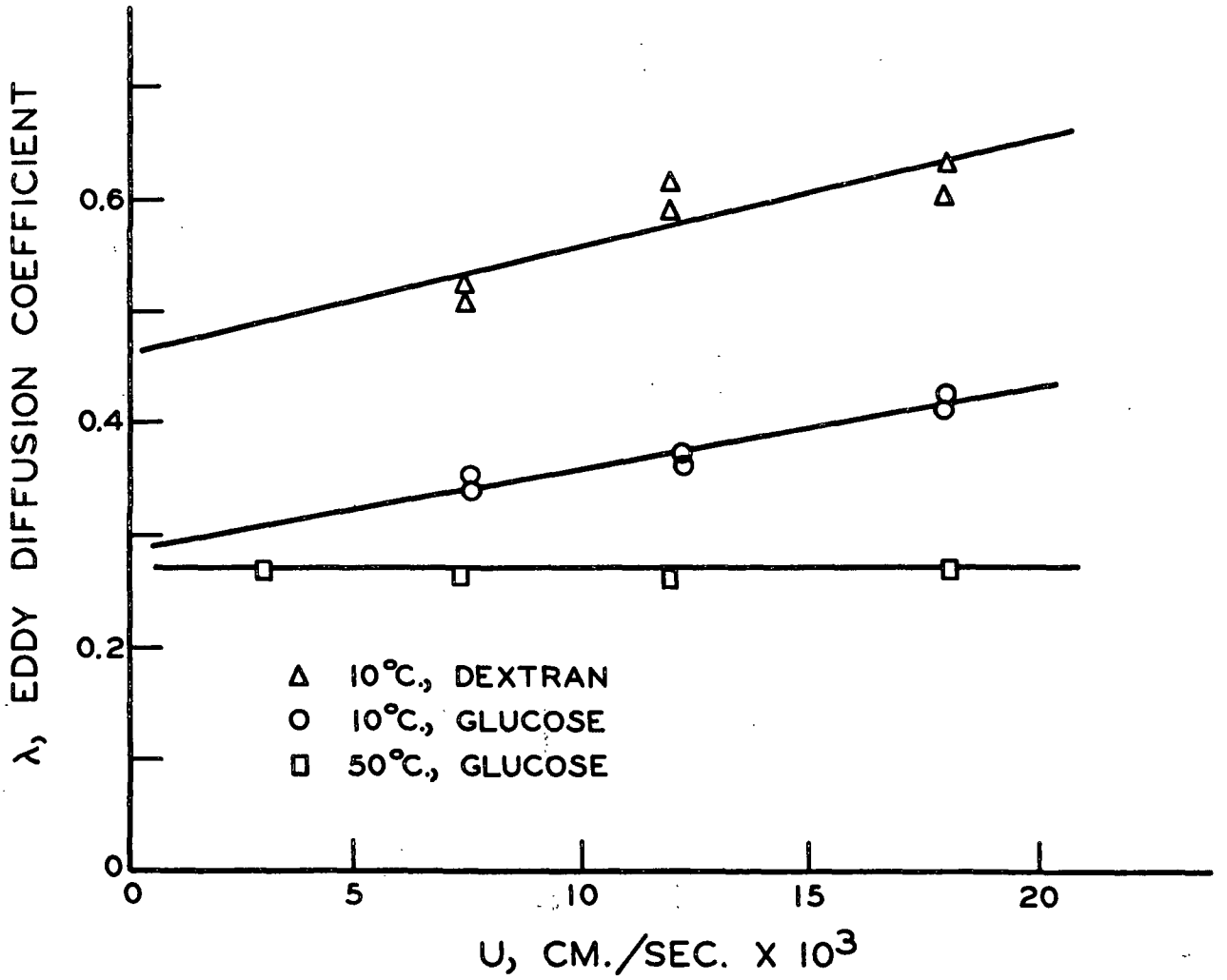

Figure 17. Axial Dispersion Data, 120 μm. Glass Beads

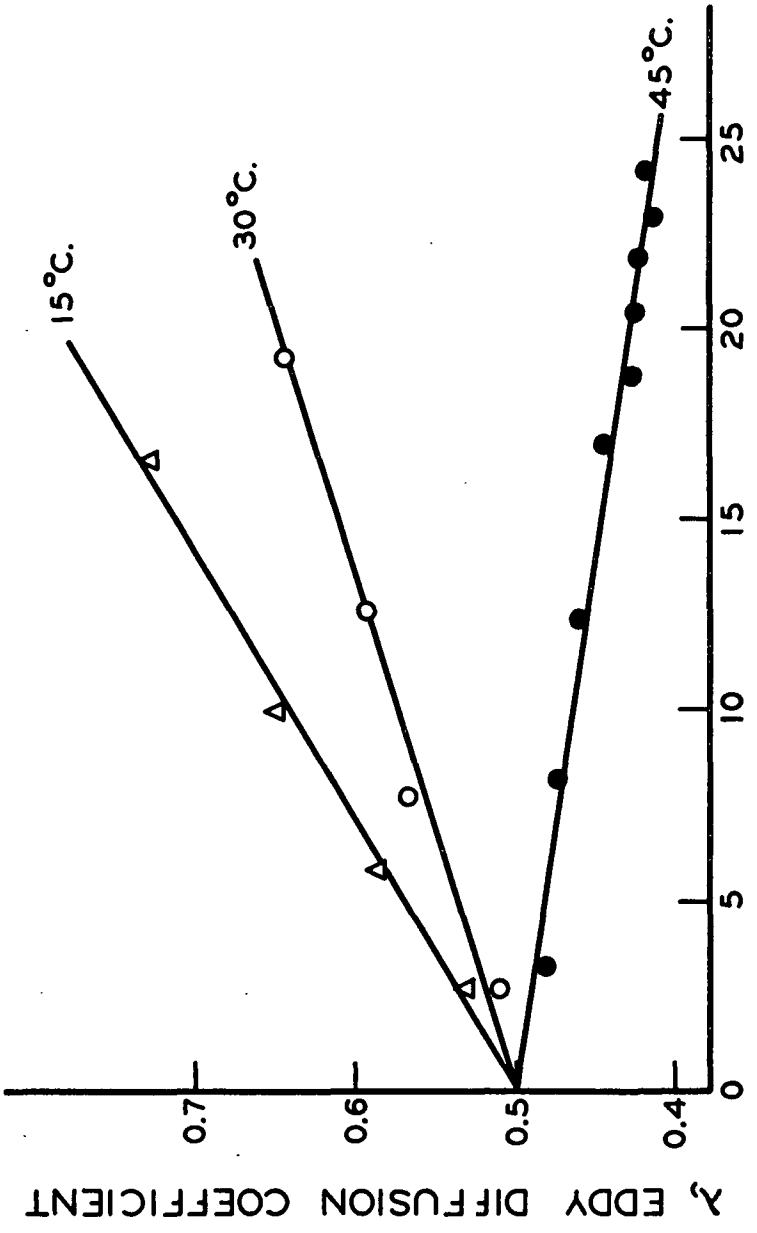

Figure 18. Normalized Axial Dispersion Data, Dextran, 70-80 Mesh P-2

where

$$C = 4\, D_m / b^2 \; d_p$$

$$1 < b < 6 \; .$$

This equation is not adequate to describe the observed axial dispersion behavior since it predicts a curvilinear relationship between H_o and U. Furthermore, the ratio C/U equals about 6×10^{-4} for typical GPC conditions. Therefore, Equation (44) would predict no velocity dependence for the experimental data shown in Fig. 17 and 18. The conclusion from this interpretation is that the random walk treatment of axial dispersion is not sufficient to describe all of the experimental observations. The deviations from the predictions were relatively small though, and for design purposes this treatment should be sufficient.

The model systems of Turner (8) would predict the general behavior described in the previous paragraphs. There has been some work done with these models (9), but there are no equations available for predictions in GPC systems. This area of analysis should be extended to provide workable equations for axial dispersion.

MASS TRANSFER

Gel phase solute transport occurs by diffusion mechanisms. Diffusivity is retarded in the hydrated gel by three mechanisms: (1) A molecule must follow a tortuous path in traveling moderate distances within the gel. (2) Only that fraction of the total cross section which is not occupied by the "solid" framework is available for diffusion. (3) The actual mobility of the molecules in the pores may be reduced by interactions with the gel matrix.

Theories for predicting retardation are very useful since gel phase diffusivity is difficult to determine experimentally. A great deal of work has been done related to diffusion in ion-exchange matrices, but success has been limited to simple, ideal

systems (14). The simplest and most widely used equations are based on statistical models for the tortuous diffusion paths inside the matrix. The most useful equations have been derived by Wheeler (61),

$$\gamma = \varepsilon_g/2 \ , \tag{45}$$

and Mackie and Meares (62),

$$\gamma = \frac{\varepsilon_g^2}{2 - \varepsilon_g} \tag{46}$$

where

$$\gamma = \underline{D}_g/\underline{D}_m \ .$$

Attempts have been made to derive equations to describe the solute-matrix interaction, but no real success has been achieved (63, 64). Table XIII shows the predictions of retardation for the gels used in this work.

TABLE XIII

PREDICTED RETARDATION RATIOS

	Equation (45)	Equation (46)
P-2	0.253	0.171
G-15	0.233	0.141
G-10	0.107	0.026

Tables XIV and XV present the experimentally determined retardation ratios. As seen in Table XIV, retardation is insensitive to temperature, but is highly dependent on the solute. Table XV compares the retardation in going from a relatively porous gel, G-16, to a less porous gel, G-10.

TABLE XIV

RETARDATION RATIOS, BIO-GEL P-2

	15°C.	30°C.	45°C.
Glucose	0.0587	0.0602	0.0671
Sucrose	0.0413	0.0492	0.0517
Raffinose	0.0307	0.0314	0.0429
Schardinger alpha-dextrin	0.0178	0.0263	0.0246
Schardinger beta-dextrin	0.0145	0.0169	0.0210

TABLE XV

RETARDATION RATIOS, SEPHADEX GELS, 20°C.

	G-15	G-10
Glycine	--	0.0228
Glycerol	--	0.0266
Glucose	0.0717	0.0160
Sucrose	0.0376	0.0090
Raffinose	0.0297	0.0065
Schardinger alpha-dextrin	0.0122	0.0024

There was a semilog correlation between retardation and molecular weight as shown in Fig. 19. The intercepts in this plot correspond reasonably well with the predictions from Equation (46). This is reasonable since the intercept value is a measure of the gel matrix contribution to the diffusivity retardation.

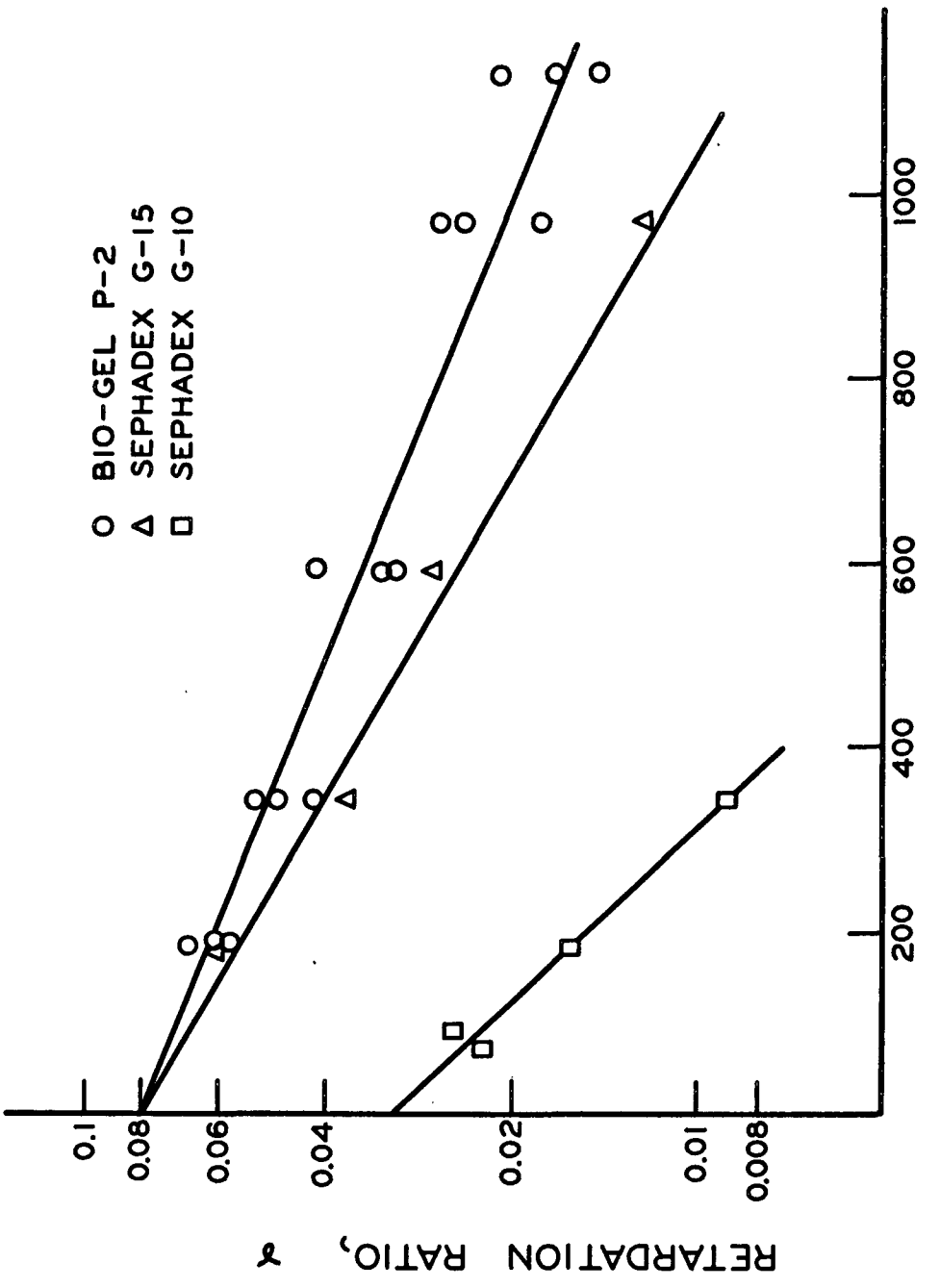

Figure 19. Retardation-Molecular Weight Correlation

As shown in Figure 19 and in Tables XIV and XV, there is a regular decrease of the retardation ratio with increasing solute molecular weight. The rapidly decreasing diffusivity is due to an increasing solute-gel interaction. The same type of interaction is responsible for the partitioning mechanism in GPC. This indicates that the mechanisms which cause solute separations on the basis of molecular size are also responsible for the velocity-dependent band spreading.

A result of the retardation-molecular weight relation is that it predicts the most band spreading for solutes which are eluted first from a GPC column — after the void volume. This is exactly opposite to the prediction made by Giddings (65) for the behavior of GPC systems. In gas chromatography and in liquid-column adsorption chromatography, the usual observation is that peaks become broader with increasing elution; however, in this work the observation was that they became narrower. This behavior is shown in Table XVI for the data: 70-80 mesh Bio-Gel P-2, 15°C., 1.18 ml./min. The volumetric standard deviation of the dextran solute is smallest because it was not partitioned.

TABLE XVI

REPRESENTATIVE SPREADING DATA

Solute	Molecular Weight	K_1	σ_v, ml.
Glucose	180	0.407	8.84
Sucrose	342	0.359	10.5
Raffinose	504	0.295	12.1
Schardinger alpha-dextrin	972	0.281	17.7
Schardinger beta-dextrin	1134	0.263	18.5
Dextran	12,000	0.0	2.94

COMPARISON OF GELS

The optimum conditions for performing a GPC separation are: (1) Temperature as high as feasible, ca. 50°C. (2) Gel particles narrowly distributed around 50 μm. diameter. (3) Flow rate around 0.01 cm./sec. These general conditions, except for the high temperature, are commonly known and will not be discussed here. Less understood are the chemical and structural properties of the gel materials which contribute to or detract from efficient GPC separations. Only two types of gel were studied in this thesis, and for this reason, the interpretations given in the following paragraphs may not apply to all types of GPC materials.

The particle shapes in the Sephadex gels were more uniform and more spherical than the Bio-Gel particles. However, there was no practical significance to this difference. The acrylamide gel was more inert than the dextran gels as exemplified by their adsorption of colored solutes. The dextran gels had a peculiar interaction with Schardinger alpha-dextrin, observed as the displacement of the distribution coefficients seen in Table XVII. The effect seems to be a property of this type of gel since it occurred for three of the gels in the Sephadex series.

TABLE XVII

EXPERIMENTAL DISTRIBUTION COEFFICIENTS, K_1

Solutes	Gels			
	P-2	G-10	G-15	G-25
Glycine	--	0.178	0.283	--
Glycerol	--	0.230	0.321	--
Glucose	0.410	0.186	0.287	0.361
Sucrose	0.361	0.136	0.241	0.328
Raffinose	0.291	0.082	0.179	0.287
Schardinger alpha-dextrin	0.271	0.119	0.289	0.371
Schardinger beta-dextrin	0.243	--	--	--

As discussed in the introduction, there are two general ways to decrease the amount of overlap between adjacent solute bands: (1) increase peak separation, and (2) decrease band spreading. The volumetric peak separation, ΔV_e, between two solutes can be written

$$\Delta V_e = \Delta K_1 \cdot V_t + V_o \quad . \tag{47}$$

Using this relationship, a gel's peak-separating efficiency can be defined on a normalized basis as

$$\text{peak separation index} = I_{ps} = -\Delta K_1/\Delta \text{ molecular weight.} \tag{48}$$

The correlation for this index is shown in Fig. 20. As seen from this plot, the correlation is good over the range most useful to carbohydrate chemists.

It is not possible to define a parameter which is directly a measure of a gel's band-spreading inefficiency. However, the indirect index,

$$\text{band spreading index} = I_{bs} = -\Delta \log \gamma/\Delta \text{ molecular weight,} \tag{49}$$

can be defined from the correlation shown in Fig. 19. It can be shown that this parameter is a normalized measure of volumetric curve variance for a gel.

The efficiency indices for the three gels are shown in Table XVIII. As seen from this data, there is little difference between the peak separation indices; P-2 better than G-15 better than G-10. There is a great deal of difference between the band-spreading indices of the gels. The lowest value of this parameter for the acrylamide gel indicates that this type of gel is intrinsically better than the two dextran gels in regard to band spreading.

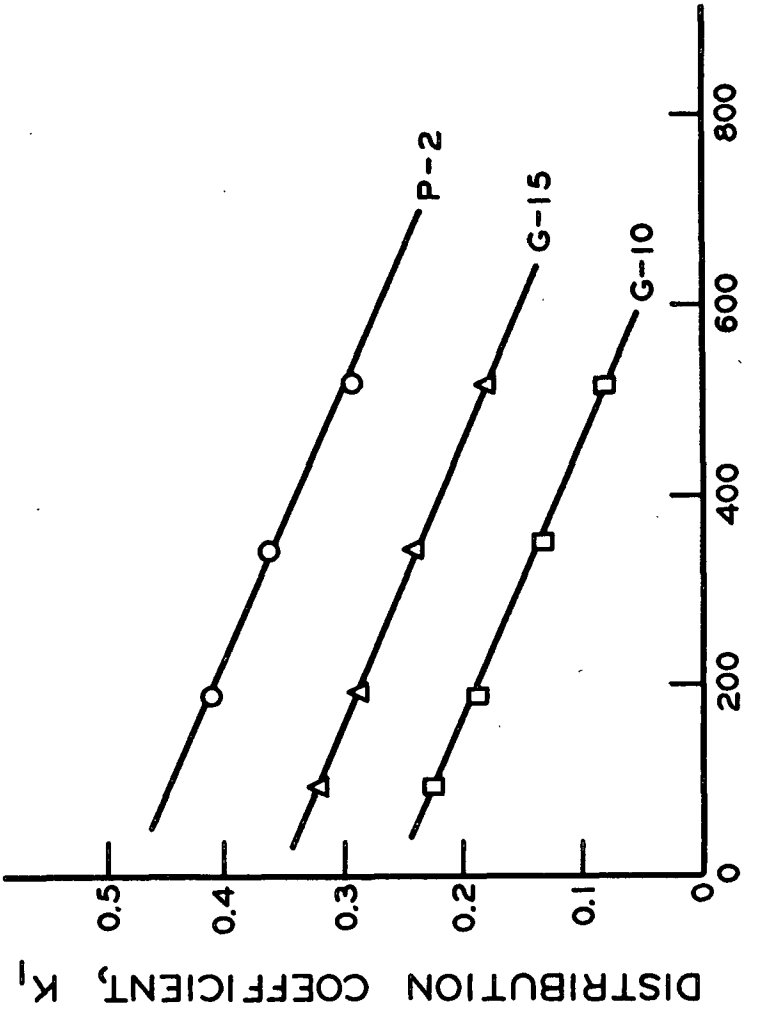

Figure 20. Peak Separation Index Correlation

TABLE XVIII

GEL EFFICIENCY PARAMETERS

Gel Type	$\underline{I}_{ps} \times 10^4$	$\underline{I}_{bs} \times 10^4$
P-2	3.65	6.07
G-15	3.54	8.67
G-10	3.50	15.9

There are two obvious differences between the gel types which may account for the behavior in the GPC systems. First, the dextran polymer is much more bulky than the acrylamide polymer. This increased "molecular surface" in the dextran gel matrix would afford more gel-solute interaction, considering other factors equal. Second, the dextran provides more hydrogen bonding sites than does the acrylamide gel. This would tend to make the solute-gel interactions stronger for the dextran gels. Thus, it would seem, the more inert a gel matrix is toward the solute, the more effective it will be in GPC applications.

CONCLUSIONS

The conclusions are based on experimental evidence from the study of three aqueous GPC systems using carbohydrate solutes. Different behavior may be found in other types of chromatography and in other GPC systems. However, by using discretion, many of the results from this work could prove useful in the analysis of other systems.

Slow gel-phase diffusion was found to control resistance to mass transport. The experimental mass transfer coefficient behaved as predicted between three gel size preparations. A linear flux expression was found to be sufficient to describe gel phase solute transport. The experimentally determined gel phase diffusion coefficients behaved as predicted by theory. Activation energies of D_g agreed with the limited amount of independent work on analogous systems. Retardation of solute diffusivity in the gel was found to be insensitive to temperature, but highly sensitive to molecular weight. A semilog correlation was found to describe this effect.

It was found that partitioning of solutes was not sensitive to eluant flow rate as has been discussed for polymer-based GPC (66). Contrary to some predictions (18, 25), a linear relationship was found between HETP and flow rate. After refinement of column packing techniques, the band-spreading behavior in the large, preparative-size column was at least equivalent to the reported behavior in much smaller, analytical-size columns. This indicates that the concept of a "reduced column diameter" (26, 27) did not apply to the systems used in this work.

Between repacked columns, the random walk theory of eddy diffusion could be applied to the observations of axial dispersion. However, it was found that this treatment was sufficient only for approximate calculations. A porosity dependence was found which was consistent with Sherman's observations of the effect of pore

size distribution on axial dispersion (10). A dependence was found upon flow rate and upon solute diffusivity. Both of these effects diminished with increasing temperature. The only explanations for these observations were found in the undeveloped theories dealing with flow through Turner structures (8).

Two uncommon diameter averages were found to best describe band spreading in GPC. Although the basis for analysis was strictly empirical, the conclusions are consistent in several avenues of logic. Axial dispersion was best described by the diameter which is equivalent to the most probable specific surface area of the particles. Slow gel diffusion can be predicted best by an average diameter which is equivalent to the most probable spherical volume of the gel particles.

GLOSSARY

A = column cross-sectional area, cm.^{2}

AV.DEV. = average deviation of a set from its mean

b = structural parameter referring to "eddy diffusion"

C = $4 D_m / b^2 d_p$

CHART = recorder chart speed, in./min.

c = final concentration of excluded solute, μg./ml.

c_g = solute concentration, gel volume basis, moles/ml.

$\langle c_g \rangle$ = average local gel phase solute concentration, moles/ml.

c_i = local interfacial solute concentration, moles/ml.

c_m = solute concentration in mobile phase, moles/ml.

c_o = initial concentration of excluded solute, μg./ml.

c_t = solute concentration, total volume basis, moles/ml.

c_∞ = solute concentration in bulk interstitial fluid, moles/ml.

D_{axial} = effective axial diffusivity, cm.^{2}/sec.

D_g = diffusion coefficient of solute in gel phase, cm.^{2}/sec.

D_m = diffusion coefficient of solute in mobile phase, cm.^{2}/sec.

$\overline{D}_g$ = defined in Equation (41)

d_p = diameter of monodispersed gel particles, cm. or μm.

d_a = area average diameter, defined Equation (36), cm. or μm.

d_n = number average diameter, defined Equation (34), cm. or μm.

d_{sps} = specific surface average diameter, defined Equation (33), cm. or μm.

d_{sv} = spherical volume average diameter, defined Equation (35), cm. or μm.

d_{wv} = weight or volume average diameter, defined Equation (37), cm. or μm.

E = average deviation

E_a = activation energy of gel-phase solute diffusion, defined in Equation (43), kcal./mole.

e = 2.71....

F = normalizing factor

$F1$ = dimensionless volumetric parameter, defined Equation (30)

$F2$ = dimensionless volumetric parameter, defined Equation (31)

GPC = abbreviation of gel permeation chromatography

H, $\tilde{H}$ = height equivalent of a theoretical plate, defined Equation (58) or Equation (59), cm.

H_e = HETP contributed by "eddy diffusion", cm.

H_o = extrapolated HETP at no flow, cm.

HCOR = HETP correction, defined Equation (32), cm.

HETP = abb. height equivalent of a theoretical plate

I_{bs} = band spreading index, defined Equation (49)

I_{ps} = peak separation index, defined Equation (48)

INCHES = chart measurement of peak elution, in.

i,j,k = indices

K_L = overall mass transfer coefficient, defined Equation (13), $sec.^{-1}$

K_1 = solute distribution coefficient, defined Equation (1), dimensionless, also Equation (6)

K_2 = solute distribution coefficient, defined Equation (2), dimensionless

k_g = mass transfer coefficient, gel volume basis, $sec.^{-1}$

k_L = mass transfer coefficient, mobile liquid basis, $sec.^{-1}$

L = measured length of column packing, cm.

L' = corrected length, cm. $L - \chi$

L_o = length of open circular tube, cm.

m = slope of line, variable dimensions

m_{gel} = mass of dry gel, g.

N = number of theoretical plates, dimensionless

N = total number of units in set

N_p = number of gel particles in set

N_g = solute flux, gel volume basis, moles $cm.^{-3}$ $sec.^{-1}$

N_{Pe} = Peclet number, defined Equation (11), dimensionless

N_t = overall solute flux, moles $cm.^{-3}$ $sec.^{-1}$

Q = volumetric eluant flow rate, ml./min. or ml./sec.

R = gas constant

S.D. = abbreviation of standard deviation

T = absolute temperature

U = interstitial fluid velocity, $Q/A\,\varepsilon$, cm./sec.

U_o = superficial fluid velocity, Q/A, cm./sec.

V = current elution volume, f (time), ml.

V_e = solute elution volume, ml.

V_f = sample feed volume to the column, ml.

V_g = column volume occupied by gel, $V_t - V_o$, ml.

V_{ig} = internal, hydrated volume of gel, ml.

V_o = void or interstitial volume of column, ml.

V_s = solution volume, ml.

V_t = total volume of column, $A\,L$, ml.

$\bar{V}_d$ = dry specific volume of gel, defined Equation (21), ml./g.

$\bar{V}_w$ = wet specific volume of gel, defined Equation (20), ml./g.

W = width of extra-column elution curve, ml.

$W1, W2$ = widths of elution curves, ml. or in.

w_r = gel water regain, defined Equation (19), dimensionless

X = solute contained in one theoretical plate, moles

z, Z = axial column dimension, cm.

α = $(1 - \sqrt{2/N})$, defined as such, dimensionless

γ = diffusivity retardation ratio, D_g/D_m, dimensionless

δ = approximate differential quantity

Δ = macroscopic difference or deviation

ε = column packing porosity, V_o/V_t, dimensionless

ε_g = gel porosity, V_{ig}/V_g, dimensionless

λ = "eddy diffusion" coefficient, defined Equation (11), dimensionless

ξ = exponent index

π = 3.1415.....

ρ = density, g./ml.

σ_t = standard deviation of elution curve, sec.

σ_v = standard deviation of elution curve, ml.

σ = standard deviation of elution curve, unspecified dimensions

Φ = collected terms of Equation (57), defined Equation (57a)

χ = length correction for sample feed volume, $V_f/2A\varepsilon$, cm.

ACKNOWLEDGMENTS

Acknowledgment is given to the thesis advisory committee: R. A. Holm, R. W. Nelson, and E. E. Dickey, for their help in evaluating and planning the thesis work.

Thanks are due the chairman of the advisory committee, Dr. Robert A. Holm, for his active involvement in the work; Ed Dickey for his learned counsel on matters chromatographic and otherwise; and Kyle Ward, Jr. and John W. Green for their participation at a critical time.

The author expresses his sincere appreciation of the contributions made by his wife, Paulette — for her assistance in the experimental work, for her critical review and preparation of manuscripts, and for her unremitting confidence.

LITERATURE CITED

1. Pharmacia Fine Chemicals, Inc. Gel filtration in theory and practice. Piscataway, N. J., Pharmacia, Dec., 1966. 56 p.

2. Laurent, T. C., and Killander, J., J. Chromatog. 14:317(1964).

3. Sun, K., and Sehon, A. H., Can. J. Chem. 43:969(1965).

4. Flodin, Per. Dextran gels and their application in gel filtration. Uppsala, Sweden, Pharmacia, 1962. 85 p.

5. Lathe, G. H., and Ruthven, C. R. J., Biochem. J. 62:665(1956).

6. Smith, W. B., and Kollmansberger, A., J. Phys. Chem. 69:4157(1965).

7. Giddings, J. C., Nature 184:357(1959).

8. Turner, G. A., Chem. Eng. Sci. 7:156(1958).

9. Aris, R., Chem. Eng. Sci. 10:80(1959).

10. Sherman, W. R., A. I. Ch. E. Journal 10:855(1964).

11. Aris, R., Chem. Eng. Sci. 7:8(1957).

12. Herdan, G. Small particle statistics. Amsterdam, Elsevier, 1953. 520 p.

13. Snyder, L. R., Anal. Chem. 39:698(1967).

14. Helfferich, Friedrich. Ion exchange. New York, McGraw-Hill, 1962. 624 p.

15. Bird, R. B., Stewart, W. E., and Lightfoot, E. N. Transport phenomena. New York, John Wiley, 1960. 780 p.

16. Carberry, J. J., A. I. Ch. E. Journal 6:460(1960).

17. Bar-Ilan, M., and Resnick, W., Ind. Eng. Chem. 49:313(1957).

18. Sie, S. T., and Rijnders, G. W. A., Anal. Chim. Acta 38:3(1967).

19. Schwartz, C. E., and Smith, J. M., Ind. Eng. Chem. 45:1209(1953).

20. Purnell, Howard. Gas chromatography. New York, John Wiley, 1962. 441 p.

21. Martin, A. J. P., and Synge, R. L. M., Biochem. J. 35:1358(1941).

22. Morris, C. J. O., and Morris, P. Separation methods in biochemistry. New York, Interscience, 1963. 887 p.

23. Hamilton, P. B., Bogue, D. C., and Anderson, R. A., Anal. Chem. 32:1782(1960).

24. Glueckauf, E., Trans. Faraday Soc. 51:34(1955).

25. Giddings, J. C., and Mallik, K. L., Anal. Chem. 38:997(1966).

26. Giddings, J. Calvin. Dynamics of chromatography. Vol. 1. New York, Marcel Dekker, 1965. 323 p.

27. Knox, J. H., Anal. Chem. 38:253(1966).

28. Tung, L. H., Moore, J. C., and Knight, G. W., J. Appl. Polymer Sci. 10:1261 (1966).

29. Scheidegger, Adrian. The physics of flow through porous media. 2d ed. London, Oxford University Press, 1960. 313 p.

30. Baddour, Raymond F., and Valbert, Jon R. Chromatographic separations. In Acrivos' Modern chemical engineering. Vol. 1. p. 487. New York, Reinhold, 1963.

31. Lapidus, L., and Amundson, N. R., J. Phys. Chem. 56:984(1952).

32. van Deemter, J. J., Zuiderweg, F. J., and Klinkenberg, A., Chem. Eng. Sci. 5:271(1956).

33. Glueckauf, E., and Coates, J. I., J. Chem. Soc. 1947:1315.

34. Glueckauf, E., Trans. Faraday Soc. 51:1540(1955).

35. Bogue, D. C., Anal. Chem. 32:1777(1960).

36. Janson, J. C., J. Chromatog. 28:12(1967).

37. Woof, J. B., and Pierce, J. S., J. Chromatog. 28:94(1967).

38. Nordstrom, C. G., Acta Chem. Scand. 21:2885(1968).

39. Saunders, D., and Pescok, R. L., Anal. Chem. 40:44(1968).

40. Swenson, Harold A. Unpublished work, 1967.

41. Tanford, Charles. Physical chemistry of macromolecules. New York, John Wiley, 1961. 710 p.

42. Spacek, P., and Kubin, M., J. Polymer Sci. Part C 16:705(1967).

43. Rickles, R. N., Ind. Eng. Chem. 58:19(1966).

44. Tuwiner, Sidney. Diffusion and membrane technology. New York, Reinhold, 1962. 421 p.

45. Granath, K., and Flodin, P., Makromol. Chem. 48:160(1961).

46. Pepper, K. W., Reichenberg, D., and Hale, D. K., J. Chem. Soc. 1952:3129.

47. Saunders, D. Personal communication, 1968.

48. Happel, J., and Brenner, H. Low Reynolds number hydrodynamics. New York, Prentice-Hall, 1965. 553 p.

49. Isenberg, Irving H. Pulp and paper microscopy. 3rd ed. Appleton, Wis., The Institute of Paper Chemistry, 1967. 214 p.

50. Jones, Alan R. An experimental investigation of the in-plane elastic moduli of paper. Doctor's Dissertation. Appleton, Wis., The Institute of Paper Chemistry, June, 1967. 137 p.

51. Perry, R. H., Chilton, C. H., and Kirkpatrick, S. D., editors. Perry's chemical engineering handbook. 4th ed. New York, McGraw-Hill, 1963.

52. Webber, R. V., J. Am. Chem. Soc. 78:536(1956).

53. Granath, K. A., J. Colloid Sci. 13:308(1956).

54. Aris, R., Chem. Eng. Sci. 9:266(1959).

55. Herdan, G. Small particle statistics. Amsterdam, Elsevier, 1953. 520 p.

56. Leva, M., Chem. Eng. 56:115(1949).

57. Golay, M. J. E. Theory of behavior. In Scott's Gas chromatography. p. 139. London, Butterworth, 1960.

58. Glasstone, S., Laider, K. J., and Eyring, H. The theory of rate processes. New York, McGraw-Hill, 1941. 875 p.

59. Horowitz, S. B., and Fenichel, I. R., J. Phys. Chem. 68:3378(1964).

60. Flodin, P., J. Chromatog. 5:103(1961).

61. Wheeler, A., Advan. Catal. 3:249(1951).

62. Mackie, J. S., and Meares, P., Proc. Roy. Soc. (London) A232:489(1955).

63. Lane, J. A., and Riggle, J. W., Chem. Eng. Progr., Symp. Ser. 55:127(1959).

64. Monet, G. P., Chem. Eng. Progr., Symp. Ser. 55:1(1959).

65. Giddings, J. C., Anal. Chem. 39:1027(1967).

66. Yau, W. W., and Malone, C. P., J. Polymer Sci., Part B 5:663(1967).

67. Glueckauf, E., Disc. Faraday Soc. 7:12(1949).

68. Glasstone, Samuel. Textbook of physical chemistry. 2d ed. New York, Van Nostrand, 1946. 1320 p.

APPENDIX I

DERIVATIONS

MATERIAL BALANCE

A short length ΔZ, of the column is used for the material balance as shown in Fig. 21. A volume, V, of effluent solution has previously passed through this layer and an additional volume, dV, is now considered.

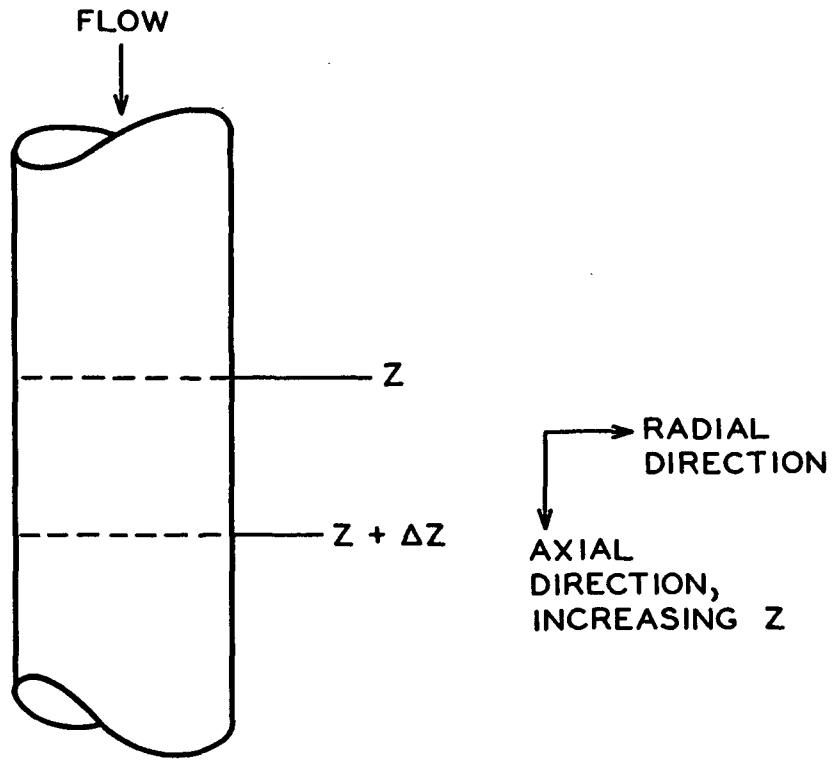

Figure 21. Column Section

Prior to the passage of dV, the layer contained $A \Delta Z c_t (V)$ moles of solute. After passage of the differential volume, the content changes to $A \Delta Z c_t (V + dv)$. The overall change in the zone is

$$d\chi = A \Delta Z \left[c_t (V + dV) - c_t (V)\right] . \qquad (50)$$

This can be written in differential form as

$$d\chi = A \Delta Z \, dV \left(\frac{\partial c_t}{\partial V}\right)_Z \quad (51)$$

Mobile phase enters the zone with a solute concentration $c_m (Z)$ and leaves with a concentration $c_m (Z + \Delta Z)$. The change in zone concentration is therefore

$$(\delta\chi)_{flow} = dV \left[c_m (Z) - c_m (Z + \Delta Z)\right] . \quad (52)$$

Taylor's theorem is then applied to this equation to give

$$(\delta\chi)_{flow} = -dV\left[\Delta Z\left(\frac{\partial c_m}{\partial Z}\right)_V + \frac{\Delta Z^2}{2}\left(\frac{\partial^2 c_m}{\partial Z^2}\right)_V\right] \quad (53)$$

The second derivative in Equation (53) was retained in Glueckauf's derivation (24).

The diffusion flux, not significant in GPC, has been given as (67)

$$(\delta\chi)_{diff} = \frac{D_m \varepsilon \, dV \, \Delta Z}{\sqrt{2}} \left(\frac{\partial^2 c_m}{\partial Z^2}\right)_V \quad (54)$$

The overall change in the zone's solute content is equal to the sum of the contributions from flow and diffusion:

$$d\chi = (\delta\chi)_{flow} + (\delta\chi)_{diff} \quad (55)$$

Substituting Equations (51), (53), and (54) into Equation (55) and after simplification, the differential mass balance is obtained:

$$\frac{D_m \varepsilon}{U\sqrt{2}} \frac{\partial^2 c_m}{\partial Z^2} = A \frac{\partial^2 c_t}{\partial V} + \frac{\partial c_m}{\partial Z} . \quad (56)$$

GFC EQUATIONS

The starting point is Equation (57) which has been derived and substantially confirmed for certain types of ion exchange chromatography (23).

$$\sigma_v^2 = 2 A^2 L \Phi \quad , \tag{57}$$

where

$$\Phi = \varepsilon(K_1 + \varepsilon)^2 \frac{D_{axial}}{U_o} + \frac{K_1^2 U_o}{K_L} \quad . \tag{57a}$$

The definition for HETP is commonly given (60) as

$$\tilde{H} = L \sigma_v^2 / V_e^2 \quad . \tag{58}$$

By using more realistic assumptions, Glueckhauf (20) was able to derive a more exact equation which rearranges to

$$H = L \frac{\sigma_v^2}{V_e^2 - \sqrt{2}\, V_e\, \sigma_v} \approx \tilde{H} \quad . \tag{59}$$

Using the relationship

$$N = L/H \quad , \tag{60}$$

Equation (59) rearranges to

$$\sigma_v^2 = V_e^2 /N - \sqrt{2}\, V_e\, \sigma_v/N \quad . \tag{61}$$

Using Equation (61) to substitute for σ_v^2 in Equation (57) and after rearrangements,

$$V_e^2/N = 2 A^2 L \Phi + \sqrt{2}\, V_e\, \sigma_v/N \quad , \tag{62}$$

or, using the relationship of Equation (60).

$$V_e^2 H/L = 2A^2 L \Phi + \sqrt{2}\, V_e\, \sigma_v/N \quad . \tag{63}$$

Making the substitutions

$$A L = V_t \tag{64}$$

and

$$\sigma_v/V_e = \sqrt{1/N} \quad , \tag{65}$$

Equation (63) rearranges to

$$H(1 - \sqrt{2/N}) = 2 \Phi V_t^2/V^2 \quad . \tag{66}$$

This reduces to

$$H\,\alpha = \frac{2\,D_{axial}}{U} + \frac{2\,K_1^2\,\varepsilon\,U}{(K_1+\varepsilon)^3\,K_L}\,, \tag{67}$$

where

$$\alpha = 1 - \sqrt{2/N}\,. \tag{68}$$

APPENDIX II

DETAILS OF MEASUREMENTS

Each data set consisted of four to six velocity runs. The pump was set to the approximate desired flow rate and the system was left operating until a steady state was approached. Thermal control of the detector head and the power supply were necessary to achieve a steady base line. Nonequilibrium in the RI monitor system was a frequent cause of base-line drift.

A solution containing a single solute was drawn into the injector valve and the injection was made. At the same time, the event was marked on the recorder. After a period of time, another solute would be injected, and so forth until all of the solutes had been injected and eluted. After all of the elution curves had been recorded, the chart was removed and the curve measurements were made.

The distance from the recorded injection to the recorded curve maximum was measured with a steel ruler and the elution volume of the solute was calculated with the equation

$$V_e = \frac{Q \text{ INCHES}}{\text{CHART}} - \text{VCOR} \qquad (69)$$

where

Q = average flow rate during elution period, $cm.^3/min.$

INCHES = distance to peak, in.

CHART = chart speed, in./min.

VCOR = dead volume correction, 3.2 $cm.^3$

V_e = elution volume, $cm.^3$.

The curve maxima were located by inspection if the peaks were sufficiently narrow. With broad curves, the method of rectilinear diameter was used (68). The center line was drawn and the peak height was measured with a ruler. The height was

divided by 2.72 and the widths at this distance were measured as indicated in Fig. 22.

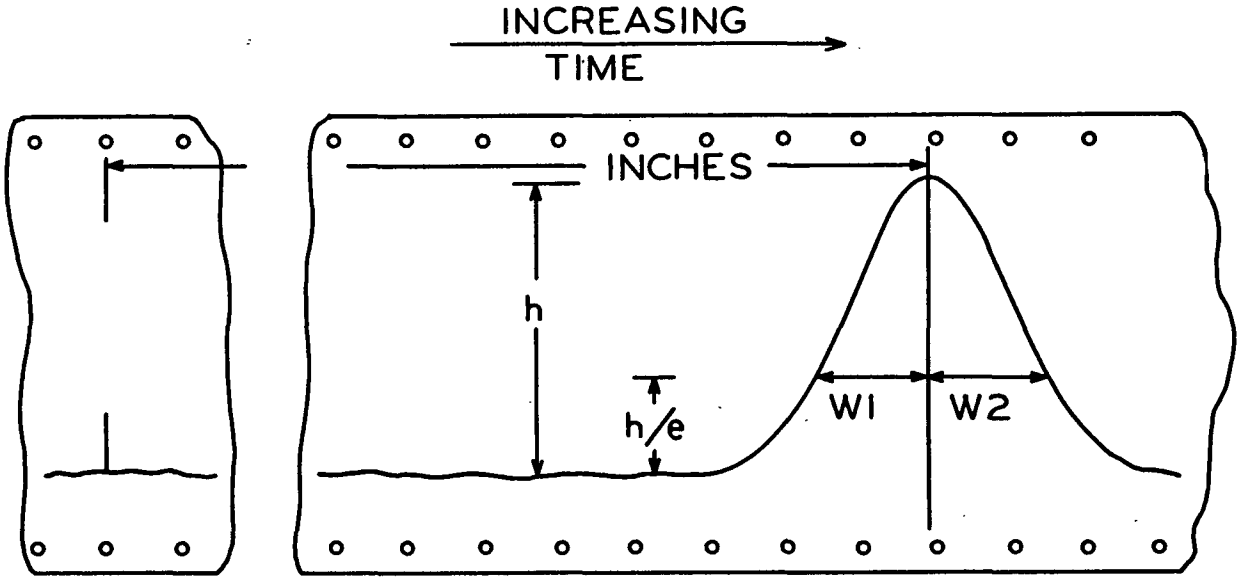

Figure 22. Curve Measurements

There were two nonideal base-line conditions encountered in the work. These are shown in exaggerated proportions in Fig. 23 along with the construction lines which were used in measuring the curve dimensions. The slant angle varied between about $\pm$ 10°, and the displacement varied between about $\pm$ 0.5 inch.

From the curve measurements, the experimental HETP was calculated from the following equations:

$$\text{HETP} = L'/N; \tag{70}$$

$$N = \frac{8\, V_e \left(V_e - \frac{W1\ Q}{\text{CHART}}\right)}{\left(\frac{(W1 + W2)\ Q}{\text{CHART}}\right)^2}\ , \tag{71}$$

$$L' = L - V_f/2\ A\ \varepsilon\ . \tag{72}$$

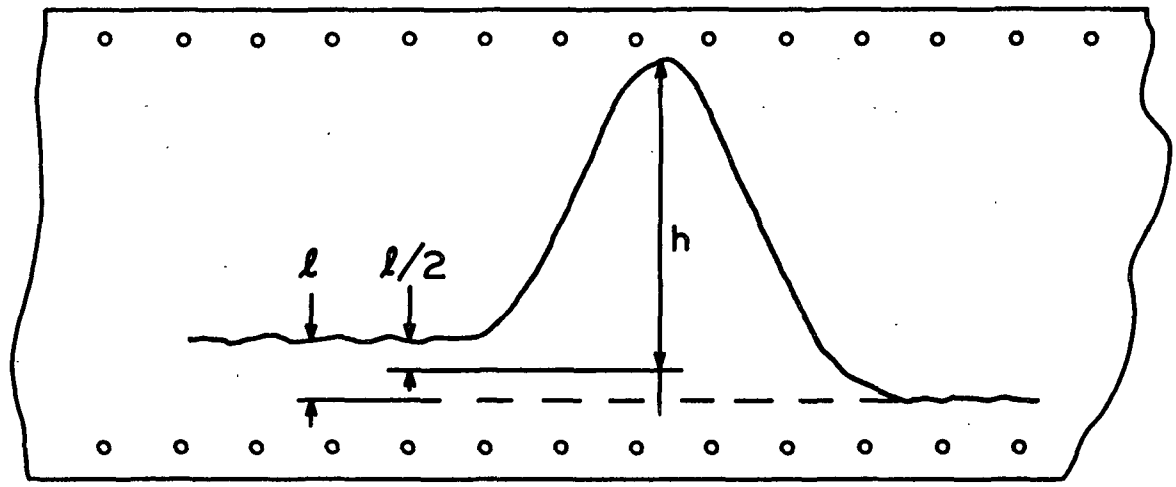

OFFSET BASE LINE

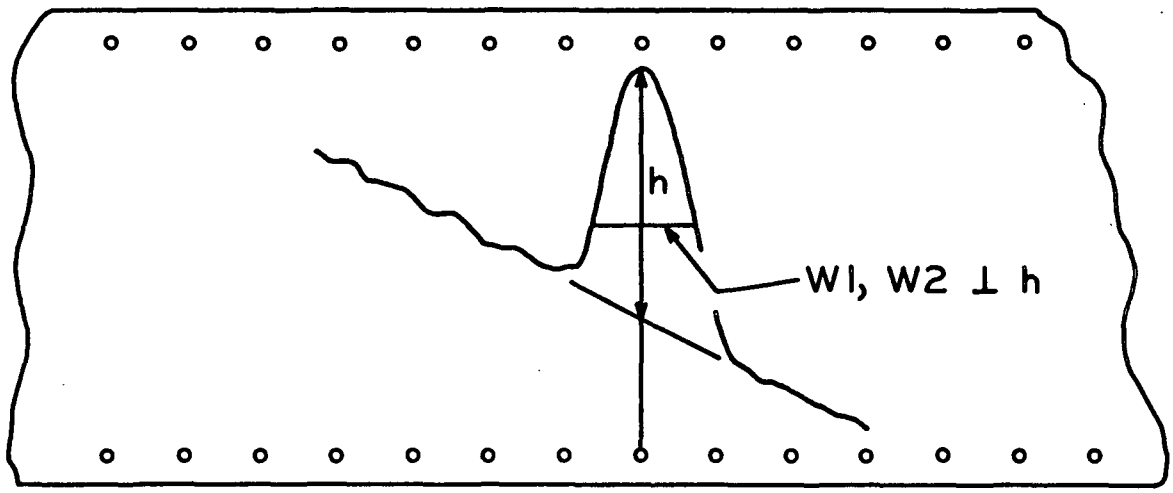

BASE-LINE SLANT

Figure 23. Nonideal Base-Line Conditions

Table XIX gives the estimated precision to which the measurements were made.

TABLE XIX

ESTIMATED PRECISION

Variable	Precision
Q	$\pm$ 0.002 $cm.^3/min.$
INCH	$\pm$ 0.02 in.
CHART	No error
VCOR	$\pm$ 0.05 $cm.^3$
Center line	$\pm$ 0.02 in.
Base line to height	$\pm$ 0.02 in.
W1, W2	$\pm$ 0.01 in.

APPENDIX III

GEL SIZE DATA

The diameter measurements of the particle samples were recorded on data cards with a digital coding microcomparator. This information was reduced by two computer programs. The first program ordered the data into a monotonically increasing set, calculated statistical parameters, and punched the ordered set of diameter measurements. The second program read the ordered data and formed diameter frequency tables. The tables were of two types — distribution by equivalent standard screen analysis and distribution by equal diameter groups. These tables could be examined graphically as histograms through auxiliary plotting programs.

The definitions of the various average diameters were given in the body of the thesis. The following additional parameters are cataloged in the following tables:

$$\text{Sum of powers} = S\xi = \sum_{i=1}^{N} d_i^{\xi} \tag{73}$$

compiled for $\xi = 1, 2, 3, 4$,

$$\text{Standard deviation of set} = \text{S. D.} = \sqrt{\frac{S2 - S1^2/N}{N}}, \tag{74}$$

$$\text{Specific Surface} = \text{SP. SURF.} = \frac{\sum_{i=1}^{N} 6/d_i}{N} . \tag{75}$$

TABLE XX

DIAMETER AVERAGES

Preparation	$\underline{d}_{sps}$, μm.	$\underline{d}_{n}$, μm.	$\underline{d}_{sv}$, μm.	$\underline{d}_{a}$, μm.	$\underline{d}_{wt.}$, μm.
100-120, P-2	104.47	116.68	125.93	134.97	141.55
70-80, P-2	123.40	143.60	158.57	173.16	182.96
50-60, P-2	133.20	170.12	204.49	240.78	263.91
Sephadex G-10	72.48	76.06	79.77	83.61	87.38
Sephadex G-15	80.97	83.74	86.79	89.97	93.36
120 μm. glass beads	115.48	122.01	125.56	128.71	130.64

TABLE XXI

STATISTICAL PARAMETERS

Preparation	N	S1, μm.	S2, $\mu m.^2$	S3, $\mu m.^3$	S4, $\mu m.^4$	S. D., μm.
100-120, P-2	1566	1.827×10^{5}	2.317×10^{7}	3.128×10^{9}	4.427×10^{11}	34.395
70-80, P-2	1550	2.226×10^{5}	3.569×10^{7}	6.181×10^{9}	1.131×10^{12}	49.042
50-60, P-2	1526	2.596×10^{5}	5.420×10^{7}	1.305×10^{10}	3.444×10^{12}	81.079
Sephadex G-10	1022	7.773×10^{4}	6.205×10^{6}	5.186×10^{8}	4.534×10^{10}	16.938
Sephadex G-15	1085	9.086×10^{4}	7.883×10^{6}	7.092×10^{8}	6.621×10^{10}	15.903
120 μm. glass beads	526	6.148×10^{4}	8.090×10^{6}	1.041×10^{9}	1.360×10^{11}	22.187

TABLE XXII

DIAMETER DISTRIBUTION, 100-120 MESH P-2

Set No.	Range of Set, μm.		Set Average	Percent By Number	Percent By Weight
1	31.7	51.0	43.8	2.49	0.10
2	51.0	70.2	62.7	8.87	1.12
3	70.2	89.5	81.2	13.92	3.78
4	89.5	108.7	99.8	15.70	7.89
5	108.7	128.0	118.8	16.85	14.26
6	128.0	147.3	137.4	21.07	27.54
7	147.3	166.5	155.5	15.45	29.23
8	166.5	185.8	172.9	4.53	11.76
9	185.8	205.1	193.5	0.83	3.02
10	205.1	224.3	214.3	0.25	1.26

TABLE XXIII

DIAMETER DISTRIBUTION, 70-80 MESH P-2

Set No.	Range of Set, μm.		Set Average	Percent By Number	Percent By Weight
1	33.8	62.6	53.0	3.80	0.14
2	62.6	91.4	77.4	15.61	1.89
3	91.4	120.2	106.2	15.93	4.86
4	120.2	149.0	133.6	13.80	8.35
5	149.0	177.8	166.4	23.29	27.13
6	177.8	206.5	191.4	19.67	34.80
7	206.5	235.3	216.9	6.19	15.92
8	235.3	264.1	247.0	1.48	5.63
9	264.1	292.9	264.5	0.06	0.29
10	292.9	321.7	307.9	0.12	0.95

TABLE XXIV

DIAMETER DISTRIBUTION, 50-60 MESH P-2

Set No.	Range of Set, μm.		Set Average	Percent By Number	Percent By Weight
1	35.9	73.2	61.9	7.07	0.20
2	73.2	110.4	92.2	23.85	2.28
3	110.4	147.7	128.5	19.33	4.90
4	147.7	184.9	163.5	10.48	5.44
5	184.9	222.2	204.1	9.56	9.59
6	222.2	259.5	242.6	11.33	19.04
7	259.5	296.7	277.6	10.41	26.21
8	296.7	334.0	311.9	5.57	19.82
9	334.0	371.2	350.0	2.03	10.22
10	371.2	408.5	389.0	0.32	2.26

TABLE XXV

DIAMETER DISTRIBUTION, SEPHADEX G-10

Set No.	Range of Set, μm.		Set Average	Percent By Number	Percent By Weight
1	31.7	42.9	39.0	0.68	0.08
2	42.9	54.1	49.6	8.41	2.05
3	54.1	65.4	59.7	17.12	7.24
4	65.4	76.6	70.9	28.66	20.34
5	76.6	87.8	82.3	22.99	25.40
6	87.8	99.0	93.0	12.42	19.81
7	99.0	110.2	103.6	6.84	15.09
8	110.2	121.5	116.4	1.95	6.09
9	121.5	132.7	126.6	0.68	2.74
10	132.7	143.9	142.8	0.19	1.12

TABLE XXVI

DIAMETER DISTRIBUTION, SEPHADEX G-15

Set No.	Range of Set, μm.		Set Average	Percent By Number	Percent By Weight
1	42.3	52.2	47.1	1.01	0.16
2	52.2	62.2	58.7	4.14	1.29
3	62.2	72.1	68.2	19.63	9.61
4	72.1	82.1	77.2	24.97	17.68
5	82.1	92.0	86.0	24.70	24.16
6	92.0	102.0	97.0	13.54	18.99
7	102.0	111.9	106.5	5.25	9.72
8	111.9	121.9	115.0	4.23	9.C
9	121.9	131.8	126.5	1.56	4.85
10	131.8	141.8	136.5	0.92	3.59

TABLE XXVII

DIAMETER DISTRIBUTION, 120 μm. GLASS BEADS

Set No.	Range of Set, μm.		Set Average	Percent By Number	Percent By Weight
1	29.6	42.9	38.0	0.57	0.01
2	42.9	56.3	51.0	1.52	0.10
3	56.3	69.6	61.5	3.23	0.38
4	69.6	82.9	77.5	2.66	0.63
5	82.9	96.3	90.2	3.23	1.20
6	96.3	109.6	103.0	6.84	3.79
7	109.6	122.9	118.4	22.05	18.59
8	122.9	136.3	130.2	38.02	42.54
9	136.3	149.6	141.2	18.25	26.01
10	149.6	162.9	154.1	3.61	6.70

APPENDIX IV

SUMMARY OF EXPERIMENTAL RUNS

The solutes glucose, raffinose, and dextran were used in all of the data runs. Additional solutes were studied in five of the runs. Data in the following tables refer to complete data runs. Elution volumes were averaged within runs to calculate the various volumetric parameters. The slope and intercept data refer to the least-squares fit of the $\underline{H}\,\alpha$ vs. $\underline{U}$ plot. The numerals which designate runs are page references to I.P.C. research notebook 2607. Table XXVIII gives the abbreviations which are used in describing the data runs. Figure 24 is a representative $\underline{H}\,\alpha$ vs. $\underline{U}$ plot.

TABLE XXVIII

ABBREVIATIONS

Abbreviation	Referent
A	50-60 Mesh Bio-Gel P-2 preparation
B	70-80 Mesh Bio-Gel P-2 preparation
C	100-120 Mesh Bio-Gel P-2 preparation
DEX	Dextran
GLU	Glucose
SUC	Sucrose
RAF	Raffinose
SAD	Schardinger alpha-dextrin
SBD	Schardinger beta-dextrin
GY	Glycine
GC	Glycerol

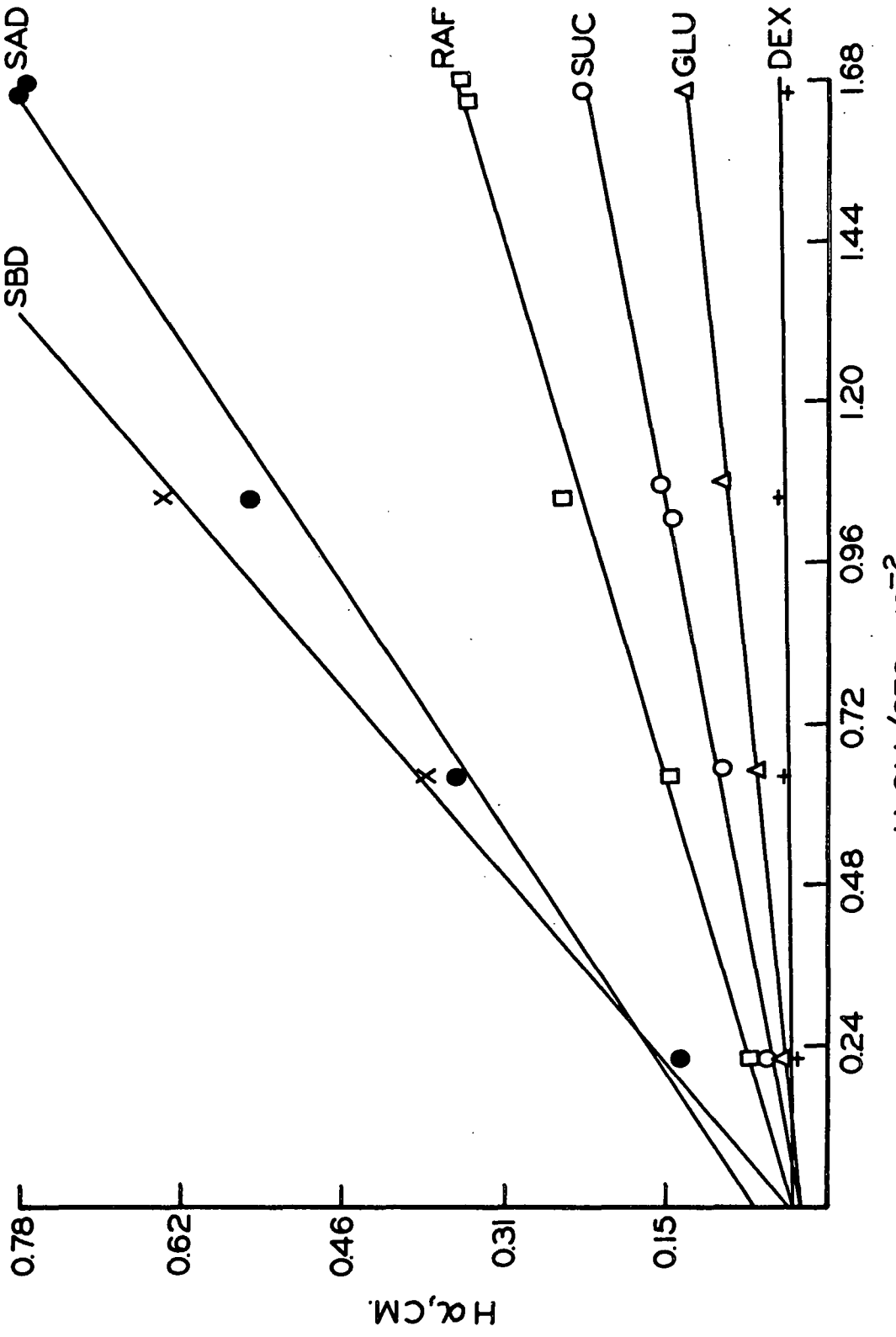

Figure 24. Representative H α vs. U Plot

TABLE XXIX

15°C. RUNS, P-2

Run	Solute	Points	Slope	Intercept	K_{-1}
14A	GLU	8	12.02	0.110	0.413
	RAF	9	27.92	0.200	0.299
	DEX	4	-17.87	0.429	--
45A	GLU	7	12.45	0.0325	0.408
	RAF	8	33.88	0.0739	0.285
	DEX	9	-0.427	0.0800	--
18C	GLU	5	2.723	0.0747	0.391
	RAF	6	12.85	0.0709	0.280
	DEX	5	1.276	0.0425	--
19C	GLU	7	4.140	0.0590	0.419
	RAF	7	14.02	0.0629	0.298
	DEX	5	2.073	0.0310	--
49C	GLU	4	4.304	0.0332	0.411
	RAF	4	14.85	0.0301	0.291
29B	GLU	5	6.929	0.0247	0.407
	SUC	5	12.84	0.0244	0.359
	RAF	5	19.86	0.0327	0.295
	SAD	5	44.16	0.0695	0.281
	SBD	2	57.19	--	0.263
	DEX	4	0.939	0.0332	--

TABLE XXX

30°C. RUNS, P-2

Run	Solute	Points	Slope	Intercept	K_{-1}
12A	GLU	4	9.516	0.0974	0.410
	RAF	5	30.22	0.0753	0.295
	DEX	5	3.765	0.0545	--
17C	GLU	5	2.742	0.0309	0.388
	RAF	5	7.537	0.0374	0.279
	DEX	4	-0.612	0.0655	--
27B	GLU	3	3.975	0.0248	0.420
	SUC	4	7.236	0.0234	0.364
	RAF	4	11.58	0.0208	0.300
	SAD	5	19.85	0.0524	0.275
	SBD	2	31.99	--	0.231
	DEX	4	0.498	0.0348	--

TABLE XXXI

45°C. RUNS, P-2

Run	Solute	Points	Slope	Intercept	K_{-1}
13A	GLU	4	4.344	0.0667	0.412
	RAF	5	11.50	0.0789	0.291
	DEX	3	-1.841	0.125	--
46A	GLU	4	5.025	0.0293	0.414
	RAF	4	11.71	0.0401	0.296
47A	GLU	2	4.891	0.0442	0.414
	RAF	2	11.76	0.0516	0.289
48A	GLU	4	4.930	0.0339	0.412
	RAF	5	11.33	0.0409	0.293
20C	GLU	7	2.057	0.0309	0.405
	RAF	7	4.687	0.0348	0.289
	DEX	6	0.946	0.0320	--
53C	GLU	10	1.110	0.0312	0.413
	RAF	7	3.997	0.0307	0.290
	DEX	5	0.030	0.0403	--
37B	GLU	9	2.667	0.0252	0.412
	SUC	10	4.868	0.0225	0.359
	RAF	8	7.246	0.0178	0.295
	SAD	7	14.96	0.0146	0.258
	SBD	2	18.33	--	0.234
	DEX	9	-0.228	0.0447	--

TABLE XXXII

20°C. RUNS, SEPHADEX GELS

Run	Solute	Points	Slope	Intercept	K_1
52, G-10	GY	3	2.153	0.0205	0.178
	GC	3	2.256	0.0178	0.230
	GLU	4	4.941	0.0195	0.186
	SUC	5	10.01	0.0194	0.136
	RAF	4	12.63	0.0335	0.0822
	SAD	3	54.02	0.3291	0.119
	DEX	4	1.114	0.0188	--
55, G-15	GLU	3	1.424	0.0228	0.287
	SUC	3	3.418	0.0241	0.241
	RAF	3	4.779	0.0360	0.179
	SAD	4	16.43	0.0786	0.289

TABLE XXXIII

COLUMN PARAMETERS

Run	Porosity	Length, cm.
12A	0.358	45.13
13A	0.354	44.65
14A	0.384	44.65
17C	0.371	48.16
18C	0.380	47.50
19C	0.398	47.26
20C	0.361	46.99
27B	0.370	49.64
29B	0.372	49.25
37B	0.378	50.03
45A	0.380	45.96
46A	0.365	46.29
47A	0.381	46.10
48A	0.368	46.30
49C	0.385	48.27
53C	0.367	48.44
52, G-10	0.365	48.96
55, G-15	0.377	48.96

APPENDIX V

DETAILS OF ERROR ANALYSIS

Each of the diameter averages was used for calculating $\underline{D_g}$ in all data sets. All of the averages were evaluated through the same method. Table XXXIV represents the data which were used for each of the diameter averages. Following this, the reduction is to a parameter which measures the consistency of the average.

TABLE XXXIV

BASIC DATA FOR EACH DIAMETER AVERAGE

Size Preparation	Glucose			Raffinose		
	15°	30°	45°	15°	30°	45°
50-60	D_{11}	D_{12}	D_{13}	D_{14}	D_{15}	D_{16}
70-80	D_{21}	D_{22}	D_{23}	D_{24}	D_{25}	D_{26}
100-120	D_{31}	D_{32}	D_{33}	D_{34}	D_{35}	D_{36}

$$\langle D_i \rangle_j = \sum_{i=1}^{3} D_{ij}/3 \tag{76}$$

$$E_j = \frac{\sum_{i=1}^{3} |\langle D_i \rangle_j - D_{ij}|}{3} \tag{77}$$

$\underline{i}$ = size preparation

$\underline{j}$ = temperature

TABLE XXXV

BETWEEN SOLUTE AND TEMPERATURE

	15°C.	30°C.	45°C.
Glucose	$E_{11}\langle D_1\rangle_1$	$E_{12}\langle D_1\rangle_2$	$E_{13}\langle D_1\rangle_3$
Raffinose	$E_{21}\langle D_2\rangle_1$	$E_{22}\langle D_2\rangle_2$	$E_{23}\langle D_2\rangle_3$

$$F_{ij} = \frac{\sum_{j=1}^{3} \langle D_i \rangle_j \ /3}{\langle D_i \rangle_j} \qquad i = 1,2 \qquad (78)$$

$$E'_{ij} = E_{ij} \cdot F_{ij} \qquad \begin{matrix} i = 1,2 \\ j = 1,2,3 \end{matrix} \qquad (79)$$

$$\langle E'_j \rangle = \sum_{i=1}^{3} E'_{ij} \ /3 \qquad j = 1,2 \qquad (80)$$

$$E''_k = \frac{\sum_{i=1}^{3} | \langle E'_j \rangle - E'_{ij} |}{3} \qquad j = k = 1,2 \qquad (81)$$

TABLE XXXVI

BETWEEN SOLUTES

	Error	Mean
Glucose	E_1''	$\langle\langle D_1 \rangle\rangle$
Raffinose	E_2''	$\langle\langle D_2 \rangle\rangle$

$$F'_k = \frac{\sum_{k=1}^{2} \langle\langle D_k \rangle\rangle}{2 \langle\langle D_k \rangle\rangle} \tag{82}$$

$$E_n''' = \sum_{k=1}^{2} E_k'' F'_k /2 \tag{83}$$

Since the actual value of D_g was not known, the error associated with each diameter was normalized for the overall average gel phase diffusion coefficient:

$$\bar{D} = \sum_{i=1}^{90} D_i/90 \tag{84}$$

$$\bar{D}_n = \sum_{j=1}^{2} \langle\langle D_j \rangle\rangle /2 \tag{85}$$

$$\Delta D_g(n) = E_n''' (\bar{D}/\bar{D}_n) \times 10^7 \tag{86}$$

The resulting values of ΔD_g are shown in Fig. 11, page 54.